# Atomic clocks and inertial sensors

Ch. J. Bordé

Abstract. We show that the language of atom interferometry provides a unified picture for microwave and optical atomic clocks as well as for gravito-inertial sensors. The sensitivity and accuracy of these devices is now such that a new theoretical framework common to all these interferometers is required that includes: (a) a fully quantum mechanical treatment of the atomic motion in free space and in the presence of a gravitational field (most cold-atom interferometric devices use atoms in "free fall" in a fountain geometry); (b) an account of simultaneous actions of gravitational and electromagnetic fields in the interaction zones; (c) a second quantization of the matter fields to take into account their fermionic or bosonic character in order to discuss the role of coherent sources and their noise properties; (d) a covariant treatment including spin to evaluate general relativistic effects. A theoretical description of atomic clocks revisited along these lines is presented, using both an exact propagator of atom waves in gravito-inertial fields and a covariant Dirac equation in the presence of weak gravitational fields. Using this framework, recoil effects, spin-related effects, beam curvature effects, the sensitivity to gravito-inertial fields and the influence of the coherence of the atom source are discussed in the context of present and future atomic clocks and gravito-inertial sensors.
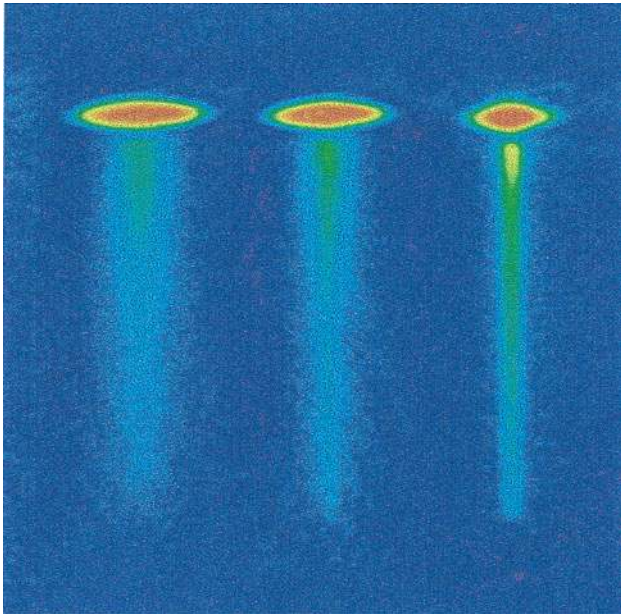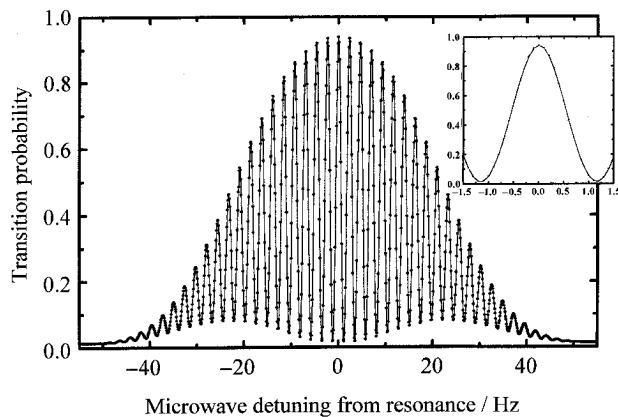

Figure 1. Rubidium atoms are extracted from a cold rubidium gas (left) and from a Bose-Einstein condensate (right). The atom beam falls down in the Earth gravity field. (*Courtesy of University of Munich [4].*)

Ch. J. Bordé: Laboratoire de Physique des Lasers, UMR 7538 CNRS, Université Paris-Nord, 99 Avenue J.-B. Clément, 93430 Villetaneuse, France; Equipe de Relativité, Gravitation et Astrophysique, LERMA, CNRS, Observatoire de Paris and Université Paris VI, 4 Place Jussieu, 75005 Paris, France; Bureau National de Métrologie, 1 Rue Gaston Boissier, 75015 Paris, France.

1. Introduction

A first goal of this paper is to clarify the link between atomic clocks and the recent field of atom interferometry [1] and to show that, indeed, microwave and optical atomic clocks are not only genuine atom interferometers [2] but also atomic inertial sensors. We demonstrate that the basic formula which gives the fringe pattern in a fountain microwave clock is the same as the corresponding formula for an atomic gravimeter. The wave character of atoms is becoming more and more manifest in these devices: the recoil energy $\hbar\delta = \hbar^2 k^2/2M$ is not negligible any more in caesium clocks ($\delta/2\pi\nu \simeq 1.5 \times 10^{-16}$). Atom sources may now be coherent sources of matter-waves (Bose-Einstein condensates [3-6], atom lasers or atomasers [7]) as illustrated in Figure 1. We have to deal with a very different picture from that of small clocks carried by classical point particles. The atomic frame of reference may not be well defined. In modern microwave atomic clocks, atoms interact twice with an electromagnetic field (this is the method of separated fields introduced by N. F. Ramsey around 1950), giving rise to interference fringes (Figure 2), which can now be reinterpreted as an interference between the de Broglie waves associated with the external motion of the atoms. Atomic clocks should thus be considered as fully quantum devices in which both the internal and external degrees of freedom must be quantized. In a first step, we recall this interpretation in the absence of gravitation.

Gravitation and inertia play a key role in slow-atom clocks, which are realized on Earth as fountains

Figure 2. Ramsey fringes obtained with the caesium fountain clock. (*Courtesy of BNM-LPTF [8].*)

(see Figure 3) and in which both interactions of atoms take place in the same resonator, once on their way up and a second time on their way down. In a second step, we thus introduce gravitation and inertia in the theory of these clocks. As the Einstein red shift and the second-order Doppler shift may become important, atomic clocks also have to be treated as relativistic devices.

Finally, we recall how the idea of separated electromagnetic (e.m.) fields in space or time has been extended to the optical domain in order to build atom interferometers, which can be used as optical clocks but also as very sensitive gravito-inertial sensors, and we outline the state of the art concerning both theory and experiments in this direction.

In the appendices, we give a complete derivation of the quantum mechanical propagator for atom waves in the presence of gravito-inertial fields and solve the Schrödinger equation for an arbitrary mode structure

of these waves. We also present an exact stationary solution of the atomic fountain and perform an explicit quantum mechanical calculation of the fringes in a fountain atomic clock for time-dependent wave packets.

2. Atom waves

The wave properties of atoms are fully described by a dispersion law relating the de Broglie frequency to the de Broglie wave vector, which is obtained from the law connecting energy $E(\overrightarrow{p})$ to momentum $\overrightarrow{p}$ by the introduction of the Planck constant. In free space (Figure 4) the corresponding curve is the hyperbola of equation
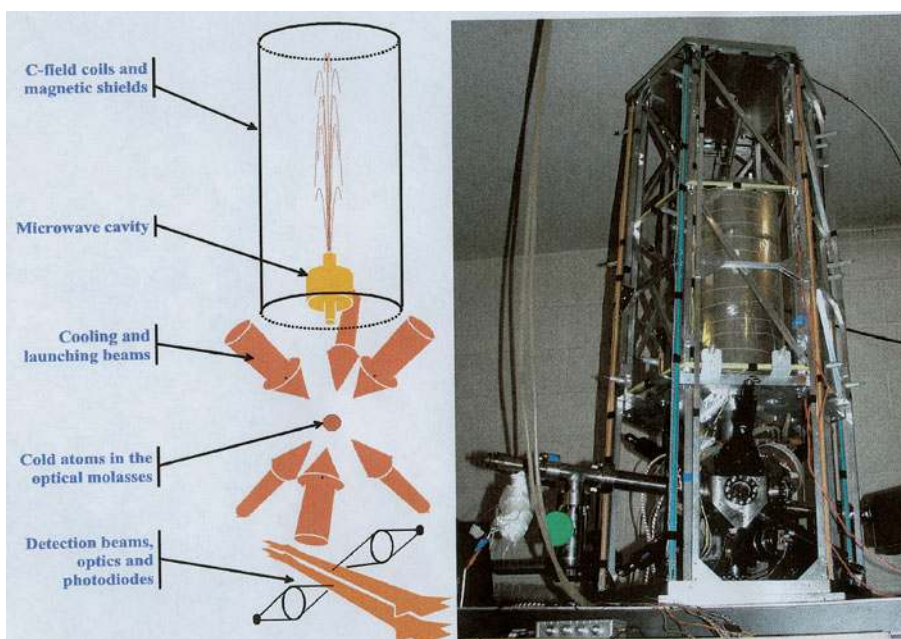
$$E(\overrightarrow{p}) = \sqrt{M^2 c^4 + p^2 c^2}. \tag{1}$$

The amplitude of an atom wave may therefore be written generally as

$$a(\overrightarrow{r}, t) = \int dE \frac{d^3 p}{(2\pi\hbar)^{3/2}} e^{i[\overrightarrow{p} \cdot (\overrightarrow{r} - \overrightarrow{r}_0) - E(t - t_0)]/\hbar}$$
$$\delta[E^2 - E^2(\overrightarrow{p})]\theta(E)a(\overrightarrow{p}, E)$$
$$= \int \frac{dE}{2E(\overrightarrow{p})} \frac{d^3 p}{(2\pi\hbar)^{3/2}}$$
$$e^{i[\overrightarrow{p} \cdot (\overrightarrow{r} - \overrightarrow{r}_0) - E(t - t_0)]/\hbar}$$
$$\delta[E - E(\overrightarrow{p})]a(\overrightarrow{p}, E), \tag{2}$$

where $\theta(E)$ is the Heaviside step function, introduced here to eliminate negative energies (antiparticles). In the non-relativistic limit:

$$a(\overrightarrow{r}, t) = \int \frac{d^3 p}{(2\pi\hbar)^{3/2}}$$
$$e^{i[\overrightarrow{p} \cdot (\overrightarrow{r} - \overrightarrow{r}_0) - (Mc^2 + p^2/2M)(t - t_0)]/\hbar} a(\overrightarrow{p}). \tag{3}$$

Figure 3. Principle and realization of a fountain clock. (*Courtesy of BNM-LPTF [8].*)
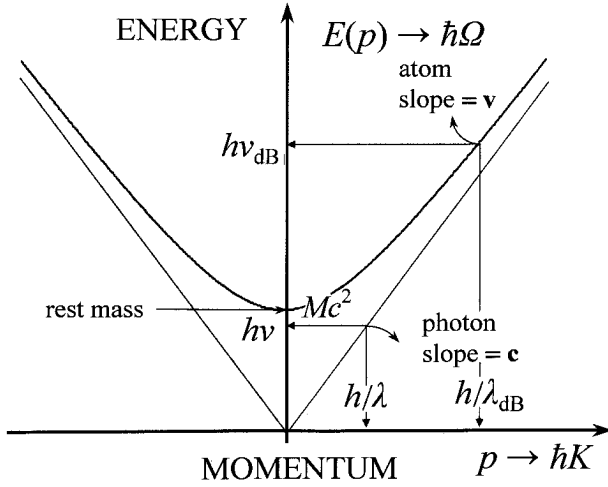
Figure 4. Energy-momentum curves: (1D cut of the mass shell) hyperbola for a massive particle, e.g. an atom in a given internal energy state, and straight lines for photons. The slope is the group velocity of the de Broglie wave.

If $a(\overrightarrow{p})$ is expanded, for example, in Hermite-Gauss functions,

$$
a(p_x, p_y, p_z) = \frac{1}{(2\pi)^{3/4}\sqrt{\Delta p_x \Delta p_y \Delta p_z}} \times
$$
$$
\sum_{lmn} H_l\left(\frac{p_x}{\sqrt{2}\Delta p_x}\right)
$$
$$
H_m\left(\frac{p_y}{\sqrt{2}\Delta p_y}\right) H_n\left(\frac{p_z}{\sqrt{2}\Delta p_z}\right)
$$
$$
\exp\left[-\frac{p_x^2}{4(\Delta p_x)^2}\right]
$$
$$
\exp\left[-\frac{p_y^2}{4(\Delta p_y)^2}\right]\exp\left[-\frac{p_z^2}{4(\Delta p_z)^2}\right],
$$
$$(4)$$

we obtain a complete orthogonal set of free-propagation modes. An even better expansion scheme is the use of 3D Hermite polynomials introduced by Grad [9] (see Appendix 2). The lowest-order modes F_{000} correspond to minimum uncertainty wave packets ($\Delta p \Delta q = \hbar/2$):

$$
a(\overrightarrow{r}, t) = \frac{\sqrt{L_x(t)L_y(t)L_z(t)}}{(2\pi)^{3/4}\sqrt{\Delta x \Delta y \Delta z}}
$$
$$
\exp\left[-L_x(t)\frac{(x-x_0)^2}{4(\Delta x)^2}\right] \qquad (5)
$$
$$
\exp\left[-L_y(t)\frac{(y-y_0)^2}{4(\Delta y)^2}\right]
$$
$$
\exp\left[-L_z(t)\frac{(z-z_0)^2}{4(\Delta z)^2}\right]e^{-iMc^2(t-t_0)/\hbar},
$$

with

$$
L_q(t) = \frac{1}{[1 + i\hbar(t-t_0)/2M(\Delta q)^2]}, \qquad (6)
$$

which can then be shifted to any frame in uniform motion by a Galilean transformation. For any higher-order mode $F_{lmn}\left[\overrightarrow{r} - \overrightarrow{r}_0, L(t)\right]$, the transposition $a(\overrightarrow{p}) \longrightarrow a(\overrightarrow{p} - \overrightarrow{p}_0)$ in (3) gives

$$
a(\overrightarrow{r}, t) = \exp\left[iS_{cl}(t, t_0)/\hbar\right]
$$
$$
\exp\{i\overrightarrow{p}_0\cdot[\overrightarrow{r} - \overrightarrow{r}_0 - \overrightarrow{p}_0(t-t_0)/M]\}
$$
$$
F_{lmn}[\overrightarrow{r} - \overrightarrow{r}_0 - \overrightarrow{p}_0(t-t_0)/M, L(t)], \qquad (7)
$$

where

$$
S_{cl}(t, t_0) = (-Mc^2 + p_0^2/2M)(t - t_0) \qquad (8)
$$

is the classical action. These free-space propagation modes transform with the same $ABCD$ law as in Gaussian laser optics [10]. The $ABCD$ matrices are functions of time in this case and we see below how the $ABCD$ law can be generalized in the presence of gravito-inertial fields.

For a travelling wave in the x direction, the δ function can be written $\delta\left(p_x - \sqrt{2ME_{kin} - p_y^2 - p_z^2}\right)$ and we may keep the kinetic energy $E_{kin} = E - Mc^2$ instead of p_x in the expression of the modes. This is a good choice if the atom wave is monochromatic, in which case the integral over energy combines with an amplitude proportional to $\delta(E_{kin} - E_0)$. In the paraxial approximation [11]:

$$
\delta\left(p_x - \sqrt{2ME_{kin} - p_y^2 - p_z^2}\right) \longrightarrow
$$
$$
\delta\left\{p_x - \sqrt{2ME_{kin}}\left[1 - \left(p_y^2 + p_z^2\right)/(4ME_{kin})\right]\right\} \quad (9)
$$

and

$$
a(\overrightarrow{r}, t) = \frac{1}{2\pi\hbar}\int dp_y dp_z a(p_y, p_z) \times
$$
$$
\exp\left[-\frac{i}{\hbar}\frac{p_y^2 + p_z^2}{2p}(x-x_0) + \frac{i}{\hbar}(p_y y + p_z z)\right] \times
$$
$$
\exp\left[\frac{i}{\hbar}p(x-x_0) - \frac{i}{\hbar}\left(Mc^2 + E_0\right)(t-t_0)\right], \qquad (10)
$$

with $p = \sqrt{2ME_0}$. The same Hermite-Gauss expansion as above may be used for $a(p_y, p_z)$. Again the propagation is described by $ABCD$ matrices, which are in this case functions of x. The lowest-order modes are then

$$
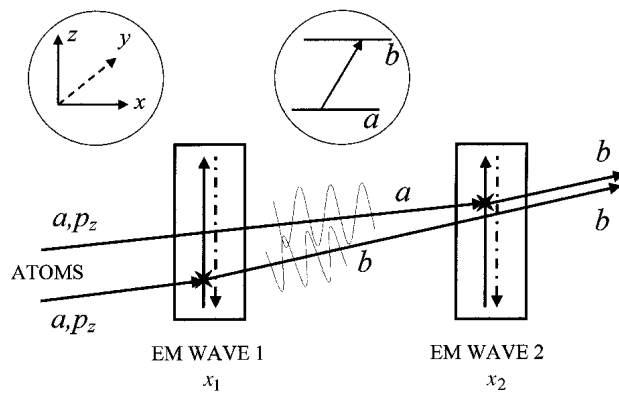a(\overrightarrow{r}, t) = \frac{\sqrt{L_y(x)L_z(x)}}{(2\pi)^{1/2}\sqrt{\Delta y \Delta z}} \times
$$

$$\exp\left[-L_y(x)\frac{(y-y_0)^2}{4(\Delta y)^2}\right]\times$$

$$\exp\left[-L_z(x)\frac{(z-z_0)^2}{4(\Delta z)^2}\right]\times$$

$$\exp\left[\frac{i}{\hbar}p(x-x_0)-\frac{i}{\hbar}\left(Mc^2+E_0\right)(t-t_0)\right] \tag{11}$$

with

$$L_q(x)=\frac{1}{[1+i\hbar(x-x_0)/2p(\Delta q)^2]}. \tag{12}$$

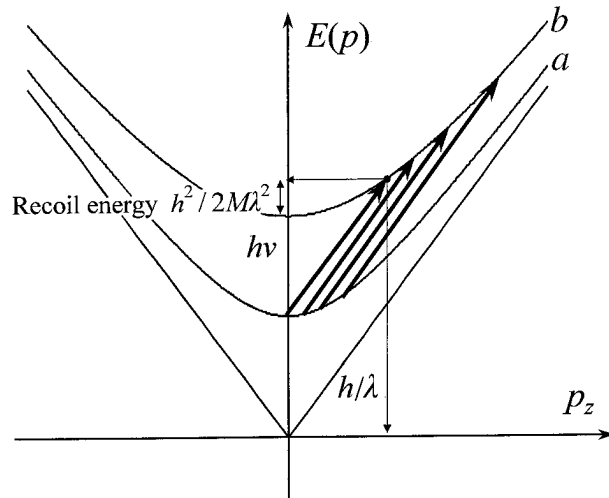## 3. Interaction of two-level atoms with electromagnetic waves

We make systematic use of energy-momentum diagrams to discuss the problem of interaction of two-level atoms with two separated field zones in a Ramsey excitation scheme (Figure 5).

Figure 6. Energy versus transverse momentum in the absorption of a photon by a two-level atom. Two different rest masses M_a, M_b correspond to the two internal energies E_a, E_b of the atom. A distribution of absorbed frequencies follows from a distribution of momenta. The central Bohr frequency is defined by $\hbar\omega_{ba}^0 = (M_b - M_a)c^2$.
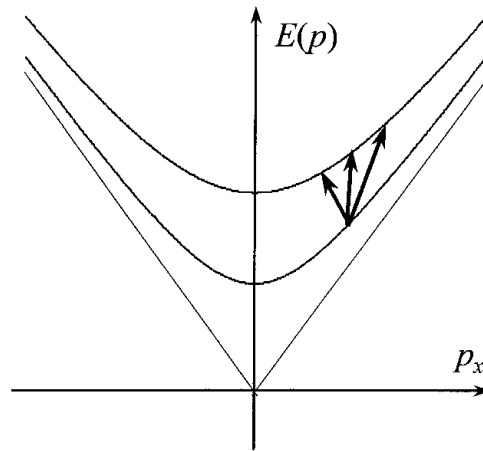

Figure 5. Illustration of the reinterpretation of the separated field method as interference between de Broglie waves. Case of successive interactions with copropagating waves.

Figures 6 and 7 illustrate the energy and momentum conservation between this two-level atom and effective photons from each travelling wave in the transverse and longitudinal directions and display the recoil energy, the first- and second-order Doppler shifts and the transit broadening. It is clear from Figure 7 that, out of resonance, an additional longitudinal momentum is transferred to the atoms in the excited state. This velocity change along the forward direction is the basis for the so-called mechanical reinterpretation of Ramsey fringes [12-15]. We now illustrate this point in more detail through a simple first-order theory of Ramsey fringes.

Let us consider a beam of two-level atoms with $E_a < E_b$ initially in state a which interacts successively with two field zones respectively centred at x_1 and x_2,

Figure 7. Energy versus longitudinal momentum in the absorption of a photon by a two-level atom. When the e.m. radiation is confined in the longitudinal direction, there is a corresponding distribution of wave vector components in that direction, which allows for a spread of absorbed frequencies (transit-time broadening or Rabi pedestal) and a change of the longitudinal momentum of the atom.

as in Figure 5, and let us calculate the excited state amplitude to first order in each field zone [2, 16]. One can check that the following expression is indeed a first-order solution of the Schrödinger equation:

$$b^{(1)}(\vec{r},t)=\frac{1}{i\hbar}\int_{-\infty}^{t}\mathrm{d}t'\int\frac{\mathrm{d}^3p}{(2\pi\hbar)^{3/2}}$$

$$\int \frac{\mathrm{d}^3 k}{(2\pi)^{3/2}} V_{ba}(\overrightarrow{k},t') e^{i\overrightarrow{k}\cdot(\overrightarrow{r}-\overrightarrow{r_1})}$$

$$e^{i[E_b(\overrightarrow{p}+\hbar\overrightarrow{k})-E_a(\overrightarrow{p})](t'-t)/\hbar}$$

$$e^{i[\overrightarrow{p}\cdot(\overrightarrow{r}-\overrightarrow{r}_0)-E_a(\overrightarrow{p})(t-t_0)]/\hbar}$$

$$\langle a|\langle \overrightarrow{p}|\Psi^{(0)}\rangle, \tag{13}$$

where the energy is given by the dispersion relation (1) and can be expanded in a Taylor series:

$$E(\overrightarrow{p}+\hbar\overrightarrow{k}) = E(\overrightarrow{p}) + \frac{\hbar\overrightarrow{k}\cdot\overrightarrow{p}c^2}{E(\overrightarrow{p})} + \frac{(\hbar k)^2 c^2}{2E(\overrightarrow{p})} + \dots$$

$$= E(\overrightarrow{p}) + \hbar\overrightarrow{k}\cdot\overrightarrow{v} + \frac{(\hbar k)^2}{2M} + \dots . \tag{14}$$

The matrix element of the Hamiltonian of interaction with the e.m. waves is $V_{ba}(\overrightarrow{r},t) = -\hbar\Omega_{ba}e^{i(\pm kz-\omega t+\varphi)}U^*(\overrightarrow{r}) + c.c.$, where Ω_{ba} is a Rabi frequency. Let us introduce a monochromatic electromagnetic wave with a Gaussian distribution of k_x (example for illustration) and, for simplicity, let us ignore the dimension y:

$$b_\pm^{(1)}(\overrightarrow{r},t) = i\Omega_{ba}e^{i(\pm kz-\omega t+\varphi)}\frac{w}{2\sqrt{\pi}}\int \frac{\mathrm{d}^3 p}{(2\pi\hbar)^{3/2}}$$

$$\int_{-\infty}^{+\infty} \mathrm{d}k_x e^{-\frac{w^2 k_x^2}{4}} e^{ik_x(x-x_1)}$$

$$e^{i(\omega-\omega_{ba}\mp kv_z - k_x v_x - \delta)(t-t_1)}$$

$$\int_{-\infty}^{t} \mathrm{d}t' e^{-i(\omega-\omega_{ba}\mp kv_z - k_x v_x - \delta)(t'-t_1)}$$

$$e^{i[\overrightarrow{p}\cdot(\overrightarrow{r}-\overrightarrow{r}_0)-E_a(\overrightarrow{p})(t-t_0)]/\hbar} a^{(0)}(\overrightarrow{p}), \tag{15}$$

with $\hbar\omega_{ba}(\overrightarrow{p}) = E_b(\overrightarrow{p}) - E_a(\overrightarrow{p}) \approx \hbar\omega_{ba}^0\sqrt{1-v^2/c^2} = \hbar\omega_{ba}(v)$ and $a^{(0)}(\overrightarrow{p}) = \langle a|\langle \overrightarrow{p}|\Psi^{(0)}\rangle$. We have used ω_{ba} as a short form for $\omega_{ba}(v)$. In the time integral, the upper bound t may be extended to infinity if the considered wave packet has left the interaction zone (this is justified in footnote 1, where the exact calculation of [11] is

---

1. The exact calculation gives

$$b_\pm^{(1)}(\overrightarrow{r},t) = i\frac{\sqrt{\pi}w\,\Omega_{ba}}{2}e^{i(\pm kz-\omega t+\varphi)}\int \frac{\mathrm{d}^3 p}{(2\pi\hbar)^{3/2}}\frac{1}{v_x}$$

$$[2e^{-w^2(\omega-\omega_{ba}\mp kv_z-\delta)^2/4v_x^2}$$

$$e^{i(\omega-\omega_{ba}\mp kv_z-\delta)(x-x_1)/v_x} - w(i\rho)]\times$$

$$e^{i[\overrightarrow{p}\cdot(\overrightarrow{r}-\overrightarrow{r}_0)-E_a(\overrightarrow{p})(t-t_0)]/\hbar} a^{(0)}(\overrightarrow{p}), \tag{16}$$

with $\rho = (x-x_1)/w_0 + i(\omega - \omega_{ba} \mp kv_z - \delta)w_0/2v_x$ and where $w(z)$ is the error function of complex arguments. The second term vanishes with the distance $(x-x_1)/w_0$, leaving the accelerated or decelerated first contribution as the dominant one.

---

recalled). We obtain a δ function expressing energy conservation as expected from the S-matrix:

$$2\pi\delta[\omega - \omega_{ba}(v) \mp kv_z - k_x v_x - \delta]$$

and corresponding to Figures 6 and 7. If the resonance condition $\omega - \omega_{ba}(v) \mp kv_z - \delta = 0$ is satisfied in Figure 6 this implies $k_x = 0$ in Figure 7, otherwise the effect of energy conservation is to select a particular component $k_x = [\omega - \omega_{ba}(v) - kv_z - \delta]/v_x$.

We obtain the first-order excited state transition amplitude:

$$b_\pm^{(1)}(\overrightarrow{r},t) = i\sqrt{\pi}e^{i(\pm kz-\omega t+\varphi)}$$

$$\int \frac{\mathrm{d}^3 p}{(2\pi\hbar)^{3/2}} \frac{w\Omega_{ba}}{v_x} e^{-w^2(\omega-\omega_{ba}\mp kv_z-\delta)^2/4v_x^2}$$

$$e^{i(\omega-\omega_{ba}\mp kv_z-\delta)(x-x_1)/v_x}$$

$$e^{i[\overrightarrow{p}\cdot(\overrightarrow{r}-\overrightarrow{r}_0)-E_a(\overrightarrow{p})(t-t_0)]/\hbar} a^{(0)}(\overrightarrow{p}) \tag{17}$$

as the product of the e.m. carrier times a Rabi frequency and a Rabi envelope, times an additional momentum phase factor for each initial wave packet Fourier component.[2] This additional longitudinal momentum is proportional to the detuning and is responsible for the Ramsey fringes, as de Broglie waves associated with each path have a different wavelength in the dark zone (Figure 5) and the transition probability integrated over the detection volume is

$$\int \mathrm{d}^3 r\, b_{1\pm}^{(1)}(\overrightarrow{r},t) b_{2\pm}^{(1)*}(\overrightarrow{r},t) \propto$$

$$\int \mathrm{d}p_z e^{-w^2(\omega-\omega_{ba}\mp kv_z-\delta)^2/2v_x^2}$$

$$e^{i(\omega-\omega_{ba}\mp kv_z-\delta)(x_2-x_1)/v_x} a^{(0)}(p_z)a^{(0)*}(p_z). \tag{18}$$

This Ramsey interference pattern has a blue recoil shift δ and is the superposition of fringe subsystems corresponding to each velocity class, shifted by the first-order Doppler effect. If the transverse velocity distribution is too broad (absence of diaphragm in the fountain) or in the optical domain, this will blur out the fringes. The integral is easily calculated for Gaussian wave packets and statistical mixtures. To make the connection with atom optics, this superposition can be rewritten as a correlation function involving the degree of transverse coherence of the atom source:

$$\int \mathrm{d}z a^{(0)}\left[z \mp \frac{\hbar k}{M}(x_2-x_1)/v_x, t\right] a^{(0)*}(z,t). \tag{19}$$

---

2. If, instead of a monochromatic non-plane (localized) wave, we had considered a plane non-monochromatic (pulsed in the time domain) wave, the exchange in momentum would have been replaced by an exchange of energy and the space-dependent phase by a time-dependent phase.

Fringes will be obtained as long as $\hbar k(x_2 - x_1)/Mv_x$ is smaller than the coherence width of the atom source.[3] This expression can be obtained directly from the previous one, using the convolution theorem, but we may also obtain it directly from the following approximate expression for $b_\pm^{(1)}(\overrightarrow{r}, t)$ which is valid for a quasi-monochromatic atom wave packet, when we neglect the v_z dependence of the Rabi envelope:

$$b_\pm^{(1)}(\overrightarrow{r}, t) = i\sqrt{\pi}e^{i(\pm kz - \omega t + \varphi)}\frac{w\Omega_{ba}}{v_x}e^{-w^2(\omega - \omega_{ba} - \delta)^2/4v_x^2}$$
$$e^{i(\omega - \omega_{ba} - \delta)(x - x_1)/v_x}$$
$$a^{(0)}\left[x - x_0, y, z \mp \frac{\hbar k}{M}(x - x_1)/v_x, t\right].$$
$$(21)$$

In the simple case of a monochromatic Gaussian wave (Mv_x stands for $\sqrt{2ME_0}$ above):

$$a^{(0)}(z - z_0, t) =$$
$$\frac{1}{(2\pi)^{1/4}\sqrt{\Delta z}[1 + i\hbar(x - x_0)/2Mv_x(\Delta z)^2]^{1/2}}$$
$$\exp\left[-\frac{(z - z_0)^2}{4(\Delta z)^2[1 + i\hbar(x - x_0)/2Mv_x(\Delta z)^2]}\right]$$

---

3. As our starting point, we could also have calculated the rate of change of the upper-state population to second order in the perturbation V, from the density matrix element $\rho_{aa}^{(0)}$, representing thermal equilibrium in the ground state (for a stationary system and whenever there is such an equilibrium within the considered degrees of freedom):

$$< b^{(1)}(\overrightarrow{r}, t)b^{(1)*}(\overrightarrow{r}, t) + c.c. >$$
$$= \frac{V_{ba}(\overrightarrow{r}, t)}{\hbar^2}\int_{-\infty}^{t}\mathrm{d}t'\int\mathrm{d}^3r'\mathrm{d}^3r''\mathcal{K}_a(\vec{r}, \vec{r}'', t - t')$$
$$\rho_{aa}^{(0)}(\vec{r}'', \vec{r}')V_{ab}(\vec{r}', t')\mathcal{K}_b^*(\vec{r}, \vec{r}', t - t') + c.c.$$
$$= \frac{V_{ba}(\overrightarrow{r}, t)}{\hbar^2}\frac{n^{(0)}h^3}{Z}\int_0^{+\infty}\mathrm{d}\tau\int\mathrm{d}^3r'\mathcal{K}_a(\vec{r}, \vec{r}', \tau - i\hbar\beta)$$
$$V_{ab}(\vec{r}', t - \tau)\mathcal{K}_b^*(\vec{r}, \vec{r}', \tau) + c.c., \quad (20)$$

where $\mathcal{K}_a$ and $\mathcal{K}_b$ are the free propagators for states a and b, $n^{(0)}$ and Z the total number density and the partition function and where $\beta = 1/k_BT$. The combination of variables in the "complex time" $\tau - i\hbar\beta$ stems from the fact that the thermal propagator or correlation function $\mathcal{K}_a(\vec{r}, \vec{r}', \tau - i\hbar\beta)$ satisfies both the Schrödinger equation $i\hbar\partial\mathcal{K}/\partial t = H\mathcal{K}$ and the Bloch equation $-\partial\mathcal{K}/\partial\beta = H\mathcal{K}$ with the same Hamiltonian. When this is the case, the thermal propagator combines the statistical properties associated with the entropy and the kinematical properties associated with the action and the conjugate variables of the energy are respectively the time and the reciprocal temperature, with Planck and Boltzmann constants as respective quanta of action and information. The thermal correlation function $\mathcal{K}_a(\vec{r}, \vec{r}', \tau - i\hbar\beta)$ describes the coherence of the atom wave packet. Its width is the thermal de Broglie wavelength h/Mu with $u = \sqrt{2k_BT/M}$ and it gives rise to the e-fold Doppler half-width ku. Incidentally, an accurate value for the Boltzmann constant k_B could be obtained through the accurate frequency measurement of a Doppler width in a gas [17]. The equation above can also be used to discuss the Lamb-Dicke-Mössbauer effect in confined atomic systems.

$$\exp\left[\frac{i}{\hbar}Mv_x(x - x_0) - \frac{i}{\hbar}\left(Mc^2 + \frac{1}{2}Mv_x^2\right)(t - t_0)\right].$$
$$(22)$$

The previous integral gives for the signal

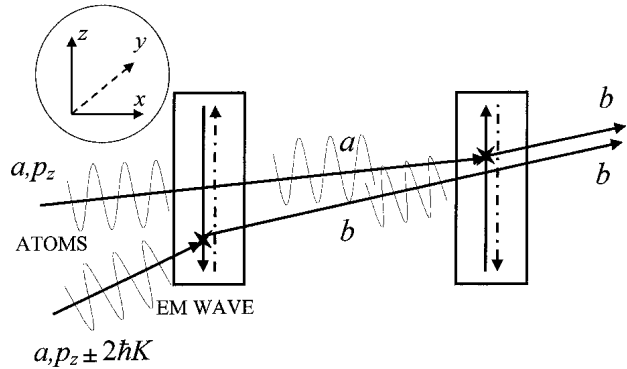$$\int\mathrm{d}^3r\, b_{1\pm}^{(1)}(\overrightarrow{r}, t)b_{2\pm}^{(1)*}(\overrightarrow{r}, t) + c.c. =$$
$$2\pi\left(\frac{w\Omega_{ba}}{v_x}\right)^2\exp\left[-\left(\frac{\hbar k}{Mv_x}\right)^2\frac{(x_2 - x_1)^2}{8(\Delta z)^2}\right]$$
$$e^{-w^2(\omega - \omega_{ba} - \delta)^2/2v_x^2}$$
$$\cos\left[(\omega - \omega_{ba} - \delta)(x_2 - x_1)/v_x + \varphi_{1\pm} - \varphi_{2\pm}\right],$$
$$(23)$$

where the second factor

$$\exp[-(\hbar k/Mv_x)^2(x_2 - x_1)^2/8(\Delta z)^2]$$

gives the loss of contrast associated with the finite coherence length.

A second mechanism, which was considered only recently for microwave clocks [18], is the interaction with oppositely travelling waves in each zone as in Figures 8 and 9.


Figure 8. Illustration of the reinterpretation of the separated field method as the interference between de Broglie waves. Case of successive interactions with counterpropagating waves.

This is possible only if the initial wave packet has Fourier components which differ by $\pm 2\hbar k$ (minimal size of atomic cloud $< \lambda_{em}$) as

$$\int\mathrm{d}z b_{1\pm}^{(1)}(\overrightarrow{r}, t)b_{2\mp}^{(1)*}(\overrightarrow{r}, t) \propto$$
$$\int\mathrm{d}z e^{\pm 2ikz}\int\mathrm{d}p_z\mathrm{d}p_z'\exp\left[i(p_z - p_z')z/\hbar\right]...$$
$$... a^{(0)}(p_z)a^{(0)*}(p_z') \Rightarrow \delta(p_z - p_z' \pm 2\hbar k). \quad (24)$$

We show that the resulting signal exhibits fringes with an opposite recoil shift $-\delta$ and that, unlike the previous one, this signal depends on the propagation
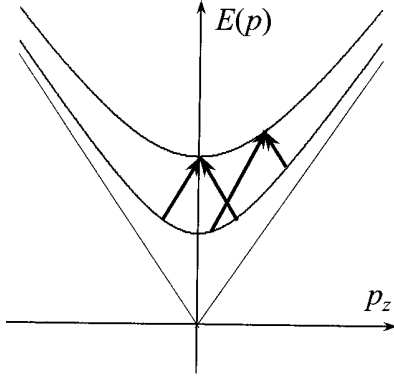
Figure 9. Energy versus transverse momentum exchanges in the case of successive interactions with counterpropagating waves.

characteristics and longitudinal coherence of the incident atom wave. If the atom wave is incoherent (e.g. in a thermal beam) we have also a $\delta(p_x - p'_x)$ in the initial density matrix. Energy conservation requires $kv_z = \mp 2\delta$ and it will not be satisfied for most velocities (Figure 9) so that the signal will tend to average out with time integration for a broad velocity distribution. In the case of a quasi-monochromatic atom wave, the integration over p'_x gives the signal as

$$\int dz b_{1\pm}^{(1)}(\overrightarrow{r}, t) b_{2\mp}^{(1)*}(\overrightarrow{r}, t) \propto$$

$$e^{i(\omega - \omega_{ba} + \delta)(x_2 - x_1)/v_x}$$

$$. \int dp_z [e^{-i(\pm kv_z + 2\delta)(2x_0 - x_2 - x_1)/v_x}$$

$$a^{(0)}(p_z) a^{(0)*}(p_z \pm 2\hbar k)], \tag{25}$$

which is strongly dependent on the position of the atom beam waist position x_0. To illustrate what happens for a coherent atom wave with a simple case, we may use here again the approximate expression of the excited state amplitude, to express this signal as

$$\int dz b_{1\pm}^{(1)}(\overrightarrow{r}, t) b_{2\mp}^{(1)*}(\overrightarrow{r}, t) \propto$$

$$\pi \left(\frac{w\Omega_{ba}}{v_x} \right)^2 e^{i(\omega - \omega_{ba} - \delta)(x_2 - x_1)/v_x} e^{-w^2(\omega - \omega_{ba} - \delta)^2/2v_x^2}$$

$$. \int dz e^{\pm 2ikz}$$

$$a^{(0)} \left(z \mp \frac{\hbar k}{M}(x - x_1)/v_x, t \right)$$

$$a^{(0)*} \left(z \pm \frac{\hbar k}{M}(x - x_2)/v_x, t \right). \tag{26}$$

For the Gaussian wave packet, the previous integral gives the signal

$$\int dz b_{1\pm}^{(1)}(\overrightarrow{r}, t) b_{2\mp}^{(1)*}(\overrightarrow{r}, t) + c.c. =$$

$$2\pi \left(\frac{w\Omega_{ba}}{v_x} \right)^2 \exp \left[-\left(\frac{\hbar k}{Mv_x} \right)^2 \frac{(2x_0 - x_2 - x_1)^2}{8(\Delta z)^2} \right]$$

$$\exp \left[-2k^2(\Delta z)^2 \right] e^{-w^2(\omega - \omega_{ba} - \delta)^2/2v_x^2}$$

$$\cos \left[(\omega - \omega_{ba} + \delta)(x_2 - x_1)/v_x + \varphi_{1\pm} - \varphi_{2\mp} \right], \tag{27}$$

where the factor $\exp \left[-2k^2(\Delta z)^2 \right]$ accounts for the requirement that the minimal size of the cloud must be smaller than the electromagnetic wavelength. The other contrast factor $\exp \left[-(\hbar k/Mv_x)^2(2x_0 - x_2 - x_1)^2/8(\Delta z)^2 \right]$ shows that if the waist is located at x_1, this second contribution will have the same magnitude as the first one and the overall recoil shift will cancel [18]. If it is focused at the midpoint $x_0 = (x_1 + x_2)/2$ (perfect time reversal), this second signal will be free of Doppler effect and will tend to dominate and impose its opposite recoil shift. The situation of $x_0 = (x_1 + x_2)/2$ could be obtained, for example, with a coherent atom wave having its waist at the top of a fountain clock, which could be achieved in a clock design such as that represented in Figure 10.
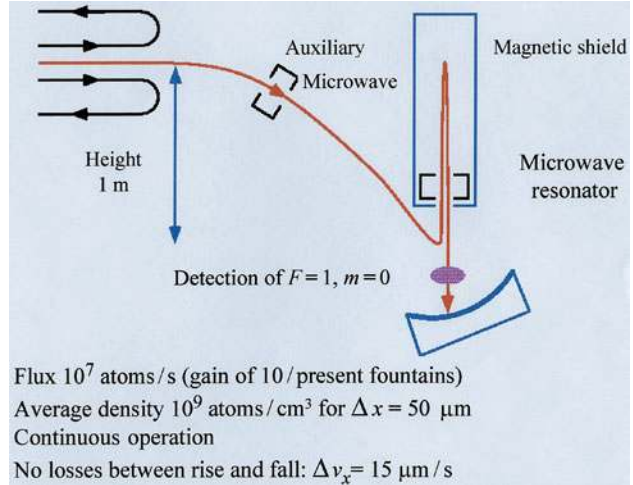
Figure 10. Schematic view of a possible future fountain clock using the continuous coherent atom wave source being developed at Laboratoire Kastler Brossel (Paris). The magnetic mirror is in the strong-field regime, in which four magnetic sublevels bounce upwards (including one connected with $F = 2$, $m = 0$), and the four others are attracted (including one connected with $F = 1$, $m = 0$). This guarantees detection on a dark background. (*Courtesy of Jean Dalibard, Christophe Salomon and David Guéry-Odelin.*)

To describe fountain geometries, which imply directly the action of the gravitational field on the atomic wave function, we now introduce gravito-inertial fields in a very general way and then apply the previous results concerning the interaction physics to the double interaction with the same microwave field.

4. Introduction of gravito-inertial fields

The well-known stationary solution of the Schrödinger equation in the presence of a gravitational field involving the Airy function [19, 20] can be extended

to the case of a continuous fountain clock [21]. This is done in Appendix 1, where the phase shifts for a two-level atom wave are derived. However, calculations with the Airy function are not so easy and we prefer to take a more general time-dependent approach, which is mathematically simpler and more powerful as most clocks use time-dependent wave packets anyway. To take gravito-inertial fields into account in the treatment of fountain clocks and other atom interferometers, we consider quite generally the Schrödinger equation obtained as the low-velocity limit of a general relativistic equation described in Section 6 of this paper:

$$i\hbar\frac{\partial|\Psi(t)\rangle}{\partial t} = \left[H_0 + \frac{1}{2M}\overrightarrow{p}_{op}\cdot\overset{\Rightarrow}{g}(t)\cdot\overrightarrow{p}_{op} - \right.$$
$$\overrightarrow{\Omega}(t)\cdot(\overrightarrow{L}_{op} + \overrightarrow{S}_{op}) -$$
$$\left. M\vec{g}(t)\cdot\vec{r}_{op} - \frac{M}{2}\vec{r}_{op}\cdot\overset{\Rightarrow}{\gamma}(t)\cdot\vec{r}_{op} + V(\vec{r}_{op},t)\right]|\Psi(t)\rangle,$$
$$(28)$$

where H_0 is an internal atomic Hamiltonian, M the corresponding rest mass operator, and $V(\vec{r}_{op},t)$ some general interaction Hamiltonian with an external field (e.g. a microwave or a laser e.m. field or the gradient of a gravitational field gradient). Gravito-inertial fields are represented by the tensors $\overset{\Rightarrow}{g}(t)$ $(=\overset{\Rightarrow}{\delta} + \overset{\Rightarrow}{h}(t)$ for a gravitational wave) and $\overset{\Rightarrow}{\gamma}(t)$ (gravitational field gradient) and by the vectors $\overrightarrow{\Omega}(t)$ and $\vec{g}(t)$. The same terms can also be used to represent the effect of various external electromagnetic fields. The operators $\overrightarrow{L}_{op} = \vec{r}_{op}\times\overrightarrow{p}_{op}$ and $\overrightarrow{S}_{op}$ are respectively the orbital and spin angular momentum operators. Apart from in $V(\vec{r}_{op},t)$, we have limited the dependence of the Hamiltonian to second order in the operators $\overrightarrow{p}_{op}$ and $\vec{r}_{op}$.

The rotation terms are easily removed with a unitary transformation (active rotation)[4] [16, 10]:

$$|\Psi(t)\rangle = U_\Omega|\Psi_0(t)\rangle, \quad (29)$$

with

$$U_\Omega(t,t_0) = \mathcal{T}\exp\left[\frac{i}{\hbar}\int_{t_0}^t\overrightarrow{\Omega}(t_1)\cdot\overrightarrow{L}_{op}dt_1\right]$$
$$\mathcal{T}\exp\left[\frac{i}{\hbar}\int_{t_0}^t\overrightarrow{\Omega}(t_1)\cdot\overrightarrow{S}_{op}dt_1\right], \quad (30)$$

---

4. In the non-rotating frame, the atomic state vector is $|\Psi_0(t)\rangle$ and an active rotation takes the e.m. wave vector from its time-independent initial position $\vec{k}$ to a time-dependent $\vec{k}_0$ rotating with the angular frequency $\overrightarrow{\Omega}(t)$. Conversely, in the rotating frame, where the e.m. wave vector is specified to be $\vec{k}$, it takes an active rotation with the angular frequency $-\overrightarrow{\Omega}(t)$ to bring the atomic state vector from $|\Psi_0(t)\rangle$ to $|\Psi(t)\rangle$.

where $\mathcal{T}$ is a chronological ordering operator. We obtain the following equation for the "non-rotating" state vector:

$$i\hbar\frac{\partial|\Psi_0(t)\rangle}{\partial t} =$$
$$\left[H_0 + \frac{1}{2M}\overrightarrow{p}_{op}\cdot\overset{\Rightarrow}{g_0}(t)\cdot\overrightarrow{p}_{op} - M\overrightarrow{g_0}(t)\cdot\vec{r}_{op} - \right.$$
$$\left. \frac{M}{2}\vec{r}_{op}\cdot\overset{\Rightarrow}{\gamma_0}(t)\cdot\vec{r}_{op} + V_0(\vec{r}_{op},t)\right]|\Psi_0(t)\rangle. \quad (31)$$

When $\overrightarrow{\Omega}$ has a fixed direction $\hat{n}$, the rotation is parametrized through the simple formula

$$\mathcal{R}(\hat{n},\theta) = \exp(i\hat{n}\cdot\vec{J}\,\theta)$$
$$= 1 + i\hat{n}\cdot\vec{J}\sin\theta - (\hat{n}\cdot\vec{J})^2(1-\cos\theta), \quad (32)$$

with $\hat{n}\theta(t) = \int_{t_0}^t\overrightarrow{\Omega}(t_1)dt_1$ and where $\vec{J}$ are the generators of infinitesimal rotations:

$$J_x = \begin{pmatrix} 0 & 0 & 0 \\ 0 & 0 & -i \\ 0 & i & 0 \end{pmatrix}, J_y = \begin{pmatrix} 0 & 0 & i \\ 0 & 0 & 0 \\ -i & 0 & 0 \end{pmatrix},$$
$$J_z = \begin{pmatrix} 0 & -i & 0 \\ i & 0 & 0 \\ 0 & 0 & 0 \end{pmatrix}. \quad (33)$$

(Matrices with the opposite sign have been used in [16]). This formula can be used to rotate all vectors and tensors and, as an example, the wave vector of the electromagnetic field transforms as

$$k = \exp(i\hat{n}\cdot\vec{J}\,\theta)k_0. \quad (34)$$

If $\overrightarrow{\Omega}$ does not have a fixed direction, a chronological ordering operator $\mathcal{T}$ must be introduced in each of these formulas and $\mathcal{R}(\hat{n},\theta)$ is replaced by the following orthogonal rotation matrix

$$\mathcal{R}(t,t') = \mathcal{T}\exp\left(i\int_{t'}^t\vec{J}\cdot\overrightarrow{\Omega}(t_1)dt_1\right). \quad (35)$$

The exact propagator $\mathcal{K}_0$ of (31) in the absence of $V(\vec{r}_{op},t)$ is derived in Appendix 2 by introducing a vector $\vec{\xi}$ such that

$$\ddot{\xi}_0 + n_0^{-1}\dot{n}_0\,\dot{\xi}_0 - n_0^{-1}\gamma_0\xi_0 - n_0^{-1}g_0 = 0, \quad (36)$$

and the $ABCD$ matrices of Gaussian optics [16, 10]:

$$\mathcal{K}_0(q,q',t,t') = \left(\frac{M}{2\pi i\hbar}\right)^{3/2}|\det B_0|^{-1/2}\exp\left[iS/\hbar\right], \quad (37)$$

where S is Hamilton's principal function:

$$S(q, q', t, t') = -E(t - t') + M \widetilde{\dot{\xi}} n (q - \xi) +$$
$$\int_{t'}^{t} L(t_1)\mathrm{d}t_1 + \frac{M}{2}\big[(\tilde{q} - \tilde{\xi})DB^{-1} (q - \xi) -$$
$$2(\tilde{q} - \tilde{\xi}) \widetilde{B^{-1}} q' + \tilde{q}' B^{-1}A q'\big], \qquad (38)$$

where $L = M(\widetilde{\dot{\xi}}n\dot{\xi} + \tilde{\xi}\gamma\xi + 2\tilde{g}\xi)/2$ is a partial Lagrangian and where $n^{-1}, \gamma, g, \Omega$ are matrices corresponding to the tensors $\overset{\Rightarrow}{g}(t), \overset{\Rightarrow}{\gamma}(t)$ and vectors $\vec{g}(t), \overrightarrow{\Omega}(t)$ (we have omitted the subscript 0 whenever unnecessary).

If n^{-1} and γ are independent of time,

$$\begin{pmatrix} A & B/t_1 \\ Ct_1 & D \end{pmatrix} = \sigma_0 \cosh\left[(n^{-1}\gamma)^{1/2}(t - t')\right] +$$
$$\vec{\sigma} \cdot \hat{u} \sinh\left[(n^{-1}\gamma)^{1/2}(t - t')\right], \qquad (39)$$

where $\hat{u} = ((n^{-1/2}\gamma^{-1/2}/t_1 + \gamma^{1/2}n^{1/2}t_1)/2, i(n^{-1/2}\gamma^{-1/2}/t_1 - \gamma^{1/2}n^{1/2}t_1)/2, 0)$ satisfies $\hat{u}^2 = I$, $\vec{\sigma}$ are the Pauli matrices and I and σ_0 are respectively (3×3) and (2×2) unit matrices. If g_0 is also independent of time,

$$\xi_0 = -\gamma_0^{-1}\Big\{1 - \cosh\left[(\gamma_0 n_0^{-1})^{1/2}(t - t')\right]\Big\}g_0. \quad (40)$$

Finally the rotation (30) is used to bring the propagator back in the rotating frame:

$$\mathcal{K}(q, q', t, t') = \mathcal{K}_0\big(\mathcal{R}^{-1}(t, t')q, q', t, t'\big)$$
$$= \mathcal{K}_0(q_0, q', t, t'). \qquad (41)$$

Using the invariance of the action S and of $|\det B|$ in this rotation, we see that the propagator $\mathcal{K}(q, q', t, t')$ has the same form as $\mathcal{K}_0$ with transformed matrices $ABCD$:

$$(A, B, C, D) = \mathcal{R}(t, t')(A_0, B_0, C_0, D_0) \qquad (42)$$

and transformed vectors and tensors:

$$(\xi, g) = \mathcal{R}(t, t')(\xi_0, g_0) \qquad (43)$$
$$(n^{-1}, \gamma) = \mathcal{R}(t, t')(n_0^{-1}, \gamma_0)\mathcal{R}^{-1}(t, t'). \qquad (44)$$

This propagator is then used to "propagate" wave packets along both arms of the interferometer. For this, we use the theorem demonstrated in Appendix 2. Let us illustrate this theorem with a simple example (without rotation). For one space dimension z, with

$$\vec{g}_0(z) = -(g - \gamma z/2)\hat{z}, \qquad (45)$$

the following result (corrected from [16]) is obtained for the wave packet at (z, t):

$$\exp\left[-\frac{i}{\hbar}E(t - t_0)\right] \exp\left[\frac{iM}{\hbar}\dot{\xi}(z - \xi)\right]$$
$$\exp\left[\frac{iM}{\hbar} \int_{t_0}^{t} (\dot{\xi}^2/2 + \gamma\xi^2/2 - g\xi)\mathrm{d}t_1\right]$$
$$\int_{-\infty}^{+\infty} \mathrm{d}z'\left(\frac{M}{2\pi i\hbar B}\right)^{1/2}$$
$$\exp\Big\{(iM/2\hbar B)[D(z - \xi)^2 - 2(z - \xi)z' + Az'^2]\Big\}$$
$$\exp[iMv_0(z' - z_0)/\hbar]F(z' - z_0, X_0, Y_0)$$
$$= \exp\left[\frac{iS_{cl}(t, t_0)}{\hbar}\right]$$
$$\exp\left\{\frac{iM}{\hbar}v(t)[z - z(t)]\right\}F(z - z(t), X(t), Y(t)), \qquad (46)$$

where

$$S_{cl}(t, t_0) = M\dot{\xi}(Az_0 + Bv_0 + \xi) -$$
$$\frac{M}{2} \int_{t_0}^{t} (\dot{\xi}^2 + \gamma\xi^2)\mathrm{d}t_1 +$$
$$\frac{M}{2}(ACz_0^2 + DBv_0^2 + 2BCz_0v_0) - E(t - t_0)$$
$$= \frac{M}{\gamma^{3/2}}\bigg[\frac{g^2}{4}(\sinh 2x - 2x) +$$
$$\frac{\gamma}{4}(v_0^2 - 2gz_0 + \gamma z_0^2)\sinh 2x +$$
$$\sqrt{\gamma}v_0(-g + \gamma z_0)\sinh^2 x\bigg] - E(t - t_0) \qquad (47)$$

is the classical action, with $x = \sqrt{\gamma}(t - t_0)$, and where

$$F(z - z_0, X_0, Y_0) = \frac{1}{\sqrt{X_0}}\exp\left[\frac{iM}{2\hbar}\frac{Y_0}{X_0}(z - z_0)^2\right] \qquad (48)$$

is a Gaussian (more generally Hermite-Gaussian) wave packet at the initial time t_0 in which the central position z_0, the initial velocity v_0 and the initial complex width parameters X_0, Y_0 in phase space, have to be replaced by their values at time t given by the $ABCD\xi$ transformation law:

$$z(t) = Az_0 + Bv_0 + \xi \quad ; \quad X(t) = AX_0 + BY_0$$
$$v(t) = Cz_0 + Dv_0 + \dot{\xi} \quad ; \quad Y(t) = CX_0 + DY_0. \qquad (49)$$

Hence the total phase factor acquired by the atomic wave packet is $\exp[iS_{cl}(t, t_0)/\hbar]$ $\exp[ip(t)(z - z(t))/\hbar]$.[5] In the limit where

---

5. The phase shift along each arm $\left\{S_{cl}(t, t_0) - [\vec{p}(t) \cdot \vec{r}(t)]_{t_0}^{t}\right\}/\hbar$ is equal to minus the time integral of the kinetic energy in the absence of a gravity field gradient.

$\gamma \rightarrow 0$, $A = D \rightarrow 1$, $B \rightarrow t - t_0$, $C \rightarrow 0$, $\xi \rightarrow -(1/2)g(t-t_0)^2$ and $S_{cl} \rightarrow -E(t-t_0) + M(t-t_0)(v_0^2 - 2gz_0 - 2gv_0(t-t_0) + 2g^2(t-t_0)^2/3)/2$.

All these results are generalized to three space dimensions in Appendix 2 with arbitrary time-dependent tensors and vectors and any modal structure of the atom waves. To include rotations and retrieve the Sagnac effect, it will be sufficient to use, in the final result, the transformed $ABCD$ matrices, vectors and tensors given above in (42), (43) and (44). In a microwave fountain clock, there is a small Sagnac effect, out of resonance, but the corresponding shift cancels for the most part for a symmetric transverse velocity (v_z) distribution or for a truly stationary e.m. wave. We return to the Sagnac effect later in this paper for the optical domain.

The application of the $ABCD\xi$ formalism to fountain clocks (Figure 11) is given in detail in Appendix 3 with the following conclusions: the additional momentum communicated after the first interaction

$$\hbar\delta k = \hbar(\omega - \omega_{ba}(v) \mp kv_z - \delta)/v_x, \quad (50)$$

combined with the path length $\xi = -(1/2)gT^2$, gives the phase shift responsible for the Ramsey fringes $\delta k\xi$ (see Figure 11). Note that this phase shift is indeed the same as in the atom gravimeter (see below) and an atom fountain clock is essentially a gravimeter with a recoil momentum communicated longitudinally proportional to the detuning. After integration over the tranverse velocity v_z, the first-order Doppler shift $\mp kv_z$ gives a reduced contrast, which depends on the focusing of the atom wave, as discussed above. The second-order Doppler shift in $\omega_{ba}(v)$ combines with the gravitational phase shift to give a correction factor $(1 + v_0^2/6c^2)$ to ω_{ba}. The final overall phase factor for the fringes is thus

$$\exp\left\{i\left[\omega - \omega_{ba}^0\left(1 + \frac{1}{6}\frac{v_0^2}{c^2}\right) - \delta\right]\left(\frac{2v_0}{g}\right)\right\}. \quad (51)$$

There is an opposite recoil correction for the contribution which comes from the successive interactions with oppositely travelling waves, with a contrast that depends on the position of the focal point of the atom wave, as discussed above in the absence of gravitation. In addition, there is a global gravitational red shift $\omega_{ba}^0(gh/c^2)$ of the fountain at altitude h. Finally, out of resonance, there is a small splitting of the wave packets as they travel along the two parabolic paths, which also leads to a reduction in contrast.

5. Optical atomic clocks

In the optical domain, more interaction zones are necessary to close the interferometer [22-24] and cancel the transverse phase shift (see Figure 12).

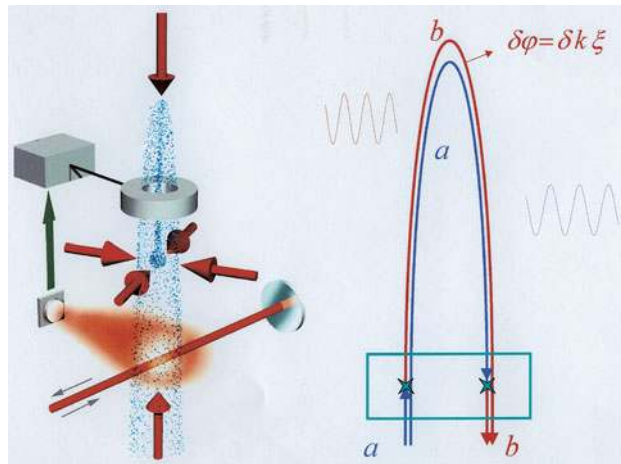This closed circuit may have different shapes [24]: parallelogram (case of three or four copropagating

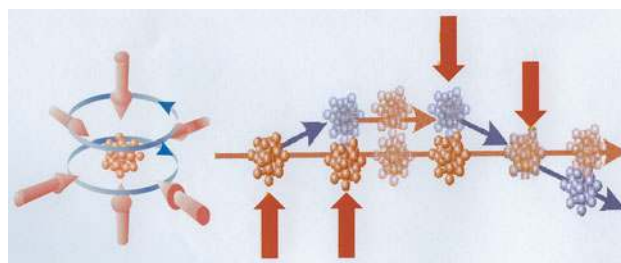
Figure 11. Phase shift in a fountain clock.

Figure 12. Magneto-optical trap (MOT, left) and sequence of four laser beam spatial zones or time pulses to generate a closed atom interferometer in space or space-time (right).
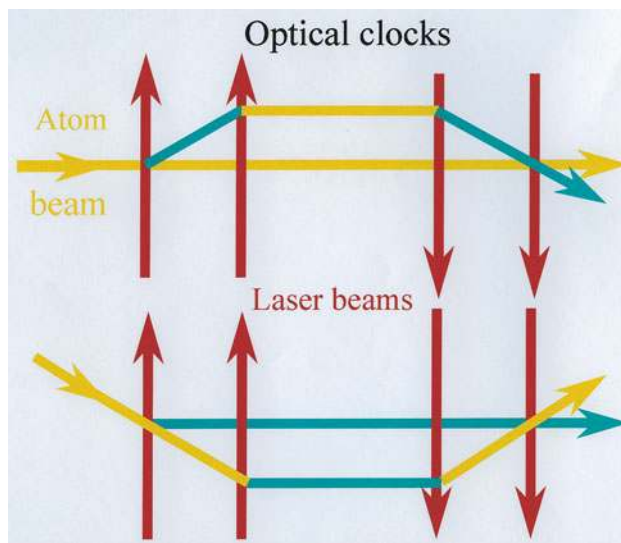

Figure 13. Pair of interferometers generated by two counterpropagating pairs of two copropagating laser beams. In one case the atoms are in their ground state in the central gap while they are in the excited state in the second interferometer central drift zone. The four interaction regions may be separated in space or in the time domain. They may involve single-photon or multiphoton (Raman or cascade) transitions.

laser beams) or trapezoid (two counterpropagating pairs of copropagating laser beams) or more complicated

geometries with larger deviations [25-27]. The choice depends on the type of phase shift that one wishes to measure: symmetric configurations are sensitive only to inertial effects while asymmetric ones also depend on the laser detuning. A variety of transition processes and effective fields may be used: single photon transitions, or two-photon transitions of Raman or cascade type [23, 24]. These interactions may be separated in space to generate a spatial interferometer [13, 28] or in time to generate a space-time interferometer, as in recent realizations of optical clocks [12, 29, 30], which use magneto-optical traps of Ca, Sr or Mg. Cold atoms are released from a magneto-optical trap and submitted to the four pulses required to generate the interferometer (Figure 13). An interference pattern such as that displayed in Figure 14 is obtained. High performances of stability and accuracy have been achieved in these different experiments. A frequency stability of $4 \times 10^{-15}/\sqrt{\tau}$ has been measured with the cold-calcium optical frequency standard compared with an ultra-stable cavity [31, 32]. The potential for improving this stability is considerable: the quantum limit for optical clocks with typical fountain parameters is $10^{-18}/\sqrt{\tau}$. Concerning accuracy, the German and US groups have achieved values of the order of 10^{-14}, presently limited by the wave-front quality of the interrogation laser, and here again this value is expected to improve significantly in the future as new techniques are being developed to further cool these atoms [33].
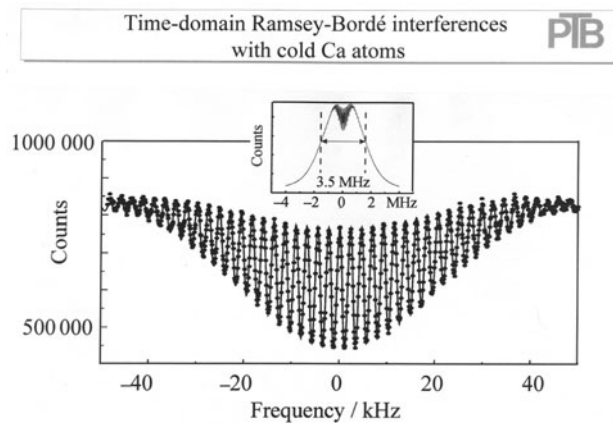

Figure 14. Interference pattern of an optical calcium clock. (*Courtesy of F. Riehle, PTB.*)

In the case of the trapezoid geometry, two different interferometers are created by two counterpropagating pairs of copropagating laser beams (Figure 15) with opposite recoil shifts. The two fringe systems are separated by 2δ. This splitting is clearly resolved in Figure 16 where the velocity distribution in a thermal beam of magnesium averages out the side fringes. In current realizations of optical clocks the fringe spacing is set precisely equal to this recoil splitting, in order to have two superimposed interference patterns as in Figure 14.

Recoil shift in optical clocks
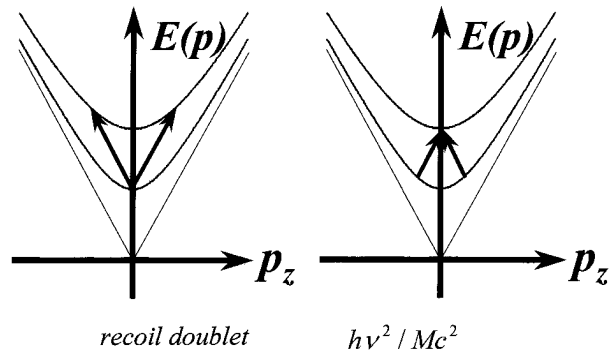
Figure 15. Energy-momentum diagrams illustrating exchanges in the two interferometers obtained with two counterpropagating pairs of two copropagating laser beams. The recoil shifts of central fringes are opposite. The first manifestation of this splitting was observed in the saturation spectrum of the methane molecule [34] and was the first quantitative demonstration of the exchange of momentum $\hbar k$ between light and an atomic species.
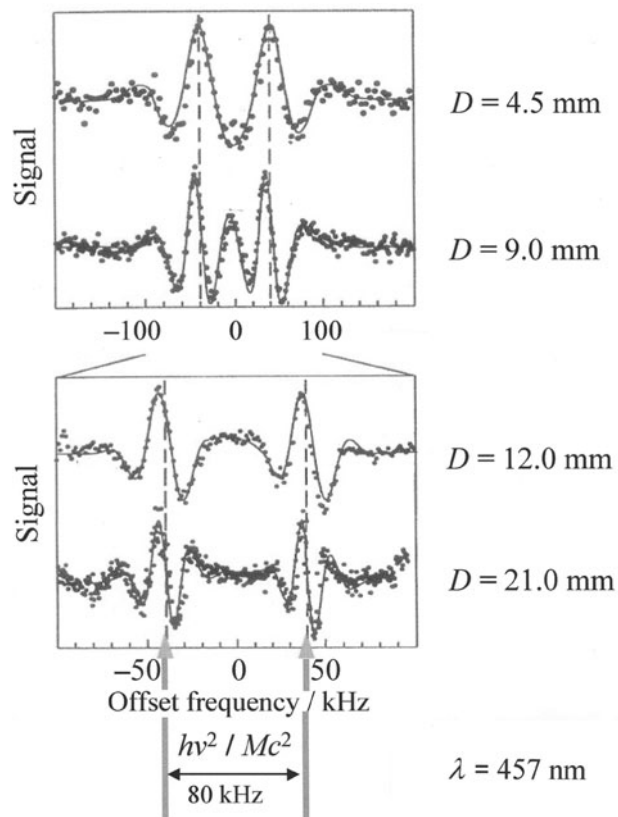
Figure 16. Interference patterns obtained with a magnesium interferometer by Ertmer's group [12]. Because of the thermal velocity distribution, only the central fringes dominate and one can see clearly the recoil splitting between the two fringe systems, with a resolution (reciprocal fringe width) increasing with the distance between the beam splitters.

In other experiments this recoil splitting is used to perform an accurate frequency measurement of $\hbar/m_{atom}$ and consequently of the fine structure constant α, thanks to the relation

$$\alpha^2 = \frac{2R_\infty}{c} \frac{m_p}{m_e} \frac{m_{atom}}{m_p} \frac{h}{m_{atom}}, \quad (52)$$

where all quantities (Rydberg constant, ratio of proton mass m_p to the electron mass m_e ...) may be known with a relative uncertainty equal to or better than 10^{-9}, which means that α may be determined directly with an uncertainty at the 10^{-9} level [27]. As the recoil shift is proportional to the difference in kinetic energies in both arms of the interferometer, it can be increased very significantly (quadratically) by an accumulation of momentum quanta $\hbar k$ on one arm with respect to the other arm [25-27, 35]. Recent determinations on Earth by Chu's group have been pushed as far as the 10^{-8} level, which is of great importance as a quantum electrodynamics (QED) test, given the discrepancies between various other determinations and independently of any QED calculation.

The theory of optical clocks began with perturbative and numerical approaches around 1977 [22]. A more sophisticated theory, which is still used to describe experimental results, introduces 2×2 $ABCD$ matrices in the internal spinor space of the two-level system and free propagation between pulses/field zones and was first published in 1982 [36, 37]. In 1990, the $ABCD\xi$ formalism for atom-wave propagation in gravito-inertial fields was presented, for the first time, in Les Houches [10]. The strong-field S-matrix treatment of the electromagnetic field zones was then published in 1994 [15, 13]. In 1995, the problem of Rabi oscillations in a gravitational field was treated in analogy/complementarity with the frequency chirp in curved wave-fronts [38, 39]. Finally, the dispersive properties of the group velocity of atom waves in strong e.m. fields were described as a generalization of the dynamical neutron diffraction theory [40] in neutron beam splitters [41-43]. Today we combine all these elements in a new sophisticated and realistic quantum description of optical clocks. This effort is also under way for atomic-inertial sensors and is essential to develop strategies to eliminate the inertial-field sensitivity of optical clocks [29]. In the next section, we outline the complete general relativistic derivation of phase shifts which was published in 1999 [44].

6. General relativistic framework for atom interferometry

It is possible to include all possible effects of inertial fields, as well as all the general relativistic effects of gravitation, in a consistent and synthetic framework [45, 41, 44], in which the atomic fields are second-quantized. The starting point is the use of coupled field equations for atomic fields of a given spin in curved space-time: e.g. coupled Klein-Gordon, Dirac or Proca equations. Gravitation is described by the metric tensor $g_{\mu\nu}$ and by tetrads, which enter in these equations. Several strategies can then be adopted: one can perform Foldy-Wouthuysen transformations [46], but conceptual difficulties arise in the case of arbitrary $g_{\mu\nu}$; one can go to the weak-field limit $g_{\mu\nu} = \eta_{\mu\nu} + h_{\mu\nu}$ with $|h_{\mu\nu}| \ll 1$ and use renormalized spinors, and finally one can consider $h_{\mu\nu}$ as a spin-two tensor-field in flat space-time [47-49] and use ordinary relativistic quantum field theory. Using this last approach, it has been possible to derive field equations that display all interesting terms, coupling Dirac atomic fields, gravitational and electromagnetic fields and simple expressions of the corresponding relativistic phase shifts in atom interferometers [44].

The evolution equation of the state vector $|\Psi(t)\rangle$ in the interaction picture is

$$i\hbar \frac{\mathrm{d}}{\mathrm{d}t} |\Psi(t)\rangle = \int \mathrm{d}^3x \ \theta^\dagger(x)\mathcal{V}_G(x)\theta(x) |\Psi(t)\rangle, \quad (53)$$

where the operator $\mathcal{V}_G(x)$, acting on the field operator $\theta(x)$, is given in compact form by

$$\mathcal{V}_G = \frac{c}{4}\alpha^\mu h_{\mu\nu} p^\nu + h.c. = \frac{c}{4}\{\alpha^\mu h_{\mu\nu}, p^\nu\}_+ \quad (54)$$

with $p^0 = -\alpha^j p_j + \gamma^0 mc$ and $p_j = i\hbar\partial_j$. $\quad (55)$

The free-field operator θ is written $\theta(x) = \sum_{r=1}^2 \int(\mathrm{d}^3p)[c_r(\overrightarrow{p})\chi^{(+)}_{\overrightarrow{p},r}(x) + d_r^\dagger(\overrightarrow{p})\chi^{(-)}_{\overrightarrow{p},r}(x)]$, where $c_r(\overrightarrow{p})$ and $d_r(\overrightarrow{p})$ are the annihilation operators for the particles or antiparticles, respectively, and $\chi^{(\pm)}_{\overrightarrow{p},r}$ are the positive or negative energy solutions of the free Dirac equation:

$$\chi^{(\pm)}_{\overrightarrow{p},r}(x) = \frac{1}{(2\pi\hbar)^{3/2}} \sqrt{\frac{Mc^2}{E(\overrightarrow{p})}} u^{(r)}_{(\pm)}(\overrightarrow{p})$$
$$e^{\mp i(E(\overrightarrow{p})t - \overrightarrow{p}\cdot\overrightarrow{r})/\hbar}. \quad (56)$$

We are interested in the output spinor corresponding to one-particle (antiparticle) states: e.g. $\psi(x) = \langle 0|\theta(x)|\Psi(t)\rangle$ for atoms. The evolution of this spinor is governed by the equation

$$i\hbar\partial_t\psi = -i\hbar c\gamma^0\gamma^j\partial_j\psi + Mc^2\gamma^0\psi + \mathcal{V}_G(x)\psi, \quad (57)$$

to which we may add terms corresponding to diagonal magnetic dipole and off-diagonal electric dipole interactions [45, 41]. This equation has been used in [41, 44] to discuss all the terms that lead to a phase shift in an interferometer.

For the phase shift, the general result is

$$\delta\varphi = -\frac{1}{\hbar}\int_{t_0}^t \mathrm{d}t' \left\{ \frac{c^2}{2E(\overrightarrow{p})} p^\mu h_{\mu\nu}(\vec{x}_0 + \vec{v}t', t')p^\nu + \right.$$

$$\frac{\gamma}{m(\gamma+1)}\left[\frac{c^2 p^\mu \vec{\nabla} h_{\mu\nu}(\vec{x}_0 + \vec{v}t', t')p^\nu}{2E^2(\vec{p})} \times \vec{p}\right]\cdot\vec{\bar{s}} -$$

$$\frac{c}{2}\left\{\vec{\nabla}\times\left[\vec{h}(\vec{x}_0 + \vec{v}t', t') - \right.\right.$$

$$\left.\left.\overset{\Rightarrow}{h}(\vec{x}_0 + \vec{v}t', t')\cdot\frac{\vec{p}c}{E(\vec{p})}\right]\right\}\cdot\vec{\bar{s}}\right\}, \tag{58}$$

where $\vec{\bar{s}}$ is the mean spin vector

$$\vec{\bar{s}} = \sum_{r,r'}\beta^*_{r,i}\beta_{r',i}\hbar w^{(r)\dagger}\vec{a}w^{(r')}/2\gamma, \tag{59}$$

where $\vec{a} = (\vec{\sigma}_\perp + \gamma\vec{\sigma}_\parallel)$ is the spatial part of the Thomas-Pauli-Lubanski 4-vector operator [50].

Expression (58) displays all the terms which may lead to a gravitational phase shift in a matter-wave interferometer:

- The terms involving h_{00} lead to the gravitational shift ($h_{00} = -2\,\vec{g}\cdot\vec{r}/c^2$), to shifts involving higher derivatives of the gravitational potential and to the analogue of the Thomas precession (spin-orbit coupling corrected by the Thomas factor).

- The terms that involve $\vec{h} = \{h^{0k}\}$ give the Sagnac effect in a rotating frame ($\vec{h} = \vec{\Omega}\times\vec{r}/c$), the spin-rotation coupling and a relativistic correction (analogous to the Thomas term for h_{00}). They also describe the Lense-Thirring effects from inertial frame-dragging by a massive rotating body, which is a source for $\vec{h}$.

- The other terms, which involve the tensor $\overset{\Rightarrow}{h} = \{h^{ij}\}$, describe genuine general relativity effects such as the effect of gravitational waves and de Sitter geodetic precession (which also includes the Thomas term for h_{00}).[6]

In fact the phase calculation is usually more complex, as (58) applies only to the case of straight unperturbed trajectories. In practice, however, one cannot ignore the fact that, when calculating the phase to first order for a given term of the Hamiltonian, the motion of the particles is affected by other terms. One example, mentioned above, is the calculation of the gravitational shift within the atom beam splitters, in which one cannot ignore the important effects of the diffracting electromagnetic field on the trajectories of the particles [41, 42, 38, 43]. Gravitational phase shifts have to be calculated along these trajectories. Another example is the gravity field itself, which, on Earth, gives parabolic trajectories for atoms. The phase shift for the other terms in (58) has to be calculated along these parabolas. A convenient way to achieve these calculations is to replace $\vec{x}_0 + \vec{v}t'$ and $\vec{v}$ in (58) by

the classical trajectory $\{\vec{x}(t'), \vec{v}(t')\}$ obtained in the $ABCD\xi$ formalism. In the non-relativistic limit, one is brought back to the Schrödinger equation and, up to second degree in position and momentum operators, the best approach is to take the full benefit of the $ABCD\xi$ formalism developed above, which gives exact results. Higher-order terms can be treated as perturbations along unperturbed trajectories.

The reader will find calculations of the phases corresponding to the various terms in [24, 23, 41, 51, 52]. In these calculations, one should never forget that the external field $h_{\mu\nu}$ acts not only on the atoms but also on other components of the experiments, such as mirrors and laser beams and that, depending on the chosen gauge, additional contributions may enter in the final expression of the phase which should, of course, be gauge independent. As an example, the Sagnac phase which can be removed from the above formula by a simple coordinate transformation will reappear in the beam-splitter phases.

The expressions valid for spins 0 and 1/2 may be conjectured to be valid for arbitrary spin if $\vec{\sigma}/2$ is replaced by the corresponding spin operator $\vec{S}$. The extension of the formulae is currently under way using higher spin formalisms.

Formula (58) also displays the analogy with electromagnetic interactions: $h_{\mu\nu}p^\nu/2$ plays the role of the 4-potential A_μ and $(E(\vec{p})/2c)\vec{\nabla}\times(\vec{h} - \overset{\Rightarrow}{h}\cdot\vec{p}c/E(\vec{p}))$ plays the role of a gravito-magnetic field $\vec{\nabla}\times\vec{A}$. This new correspondence between the gravitational interaction and the electromagnetic interaction generalizes the so-called gravito-electric and gravito-magnetic interactions introduced by DeWitt [53] and Papini [54].

The spin-independent part of this phase shift (Linet-Tourrenc [55] term) $(c^2/2E(\vec{p}))p_\mu h^{\mu\nu}p_\nu$ (a combination that also appears in the generalized Thomas precession), corresponds to $u_\mu A^\mu/\gamma$, where u_μ is the 4-velocity p_μ/M and the corresponding circulation of potential takes the form of the Aharonov-Bohm phase formula $\oint A^\mu dx_\mu$. Using Stokes theorem in four dimensions, this integral gives the phase shift as the ratio of the flux of gravito-electromagnetic forces through the interferometer space or space-time area to a quantum of flux of force $\hbar$ or $\hbar c$:

$$-\hbar\delta\varphi = \oint\frac{c^2}{2E(\vec{p})}p^\mu h_{\mu\nu}p^\nu dt = \oint\frac{1}{2}p^\mu h_{\mu\nu}dx^\nu$$

$$= \frac{1}{2}\iint d\sigma^{\mu\nu}(\partial_\mu A_\nu - \partial_\nu A_\mu),$$

with $A_\nu = \frac{1}{2}p^\mu h_{\mu\nu}$ \tag{60}

in analogy with electromagnetism. This formula gives

$$\delta\varphi = -\vec{k}\cdot\vec{g}\,T^2 \tag{61}$$

for the gravitational phase shift [23, 24] as the flux of a gravito-electric field $-c^2\vec{\nabla}h_{00}/2 = \vec{g}$ through a space-time area (which is the case above for the fountain

---

6. Some authors reserve the name "Thomas precession" for the contribution arising specifically from an acceleration $\vec{a}$ (which has been included here in h_{00}) and separate it from de Sitter precession.
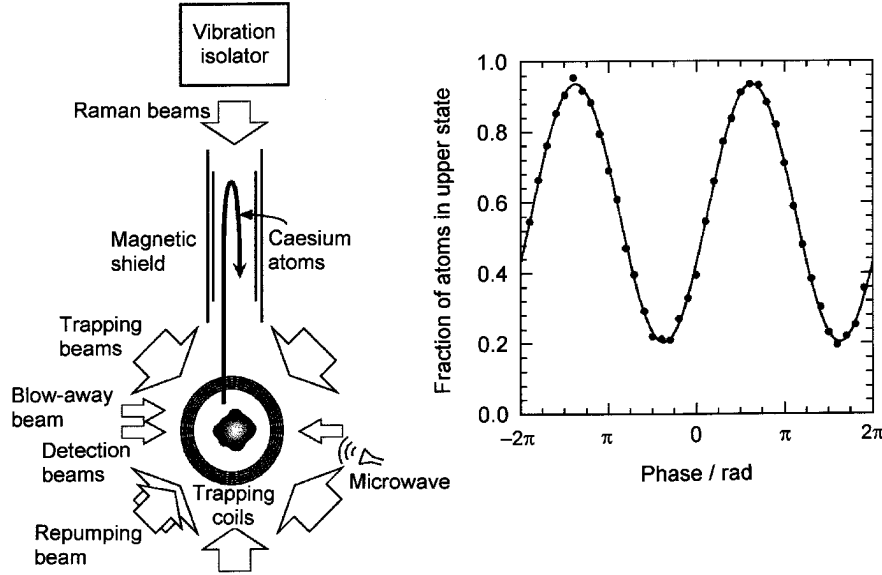
Figure 17. Atom-wave gravimeter developed at Stanford University by Chu and co-workers [56]. 5×10^8 caesium atoms extracted from a low-pressure background vapour are loaded in a MOT in 600 ms and launched upwards. A sequence of microwave, velocity-sensitive Raman and state-selective blow-away pulses places 3×10^6 atoms in the $6\,\mathrm{S}_{1/2}\ F = 3,\ M_F = 0$ state with an effective vertical temperature of approximately 10 nK. The atomic cloud enters a magnetically shielded region and is illuminated by the sequence $\pi/2 - \pi - \pi/2$ of interferometer Raman pulses which enter from below. The retromirror is vibration-isolated with an actively stabilized system. The plot at right displays typical fringes for $T = 160$ ms. Each point corresponds to a single launch of the atoms separated by 1.3 s and the data were taken over 1 min.

clock), whereas the Sagnac phase shift[7] is the flux of a gravito-magnetic field $c^2 \vec{\nabla} \times \vec{h} = 2c\vec{\Omega}$ through an area $\vec{A}$ in space [23, 24], which atomic clocks usually do not have:

$$\delta\varphi = \frac{2c\vec{\Omega} \cdot \vec{A}}{\hbar c/M}. \tag{62}$$

The spin-rotation term is discussed in more detail in [41, 44]. Its effect on atomic clocks needs to be carefully evaluated as, unlike the magnetic field, the gravito-magnetic field cannot be shielded.

7. State of the art for gravito-inertial sensors

To emphasize the sensitivity of atom interferometers to inertial and gravitational fields, a short overview of realizations of gravito-inertial sensors, including gravimeters, gradiometers and atomic gyros, is proposed in this last section. A first very successful application of atom interferometry is gravimetry and was developed by Chu and collaborators (Figure 17). This is an extension of the celebrated COW experiments for neutrons [57] to the atom world. In 1991, in one of the early experiments of atom interferometry [58], this group

demonstrated a resolution of 3×10^{-8} for g in 40 min integration time. In recent Earth gravity measurements, the relative sensitivity is $\delta g/g \simeq 3 \times 10^{-9}$ after 60 s and the absolute uncertainty is 5×10^{-9} [27, 56]. This resolution is sufficient to see clearly the effect of ocean loading on the Earth tides. Also, the agreement with a conventional corner-cube gravimeter (FG5) is at the $7 \times 10^{-9} g$ level, which constitutes by itself a test of the equivalence principle between an atomic species and a macroscopic object at that level. The corresponding space-time diagram is given in Figure 18, from which the following phase shift is calculated with the $ABCD\xi$ formalism [16]:

$$\begin{aligned}
\delta\varphi &= -k[(z_2 + z_2')/2 - z_1 - z_1' + z_0] \\
&= -\frac{k}{\sqrt{\gamma}} \Bigg(\{\sinh[\sqrt{\gamma}(T + T')] - \\
&\quad 2\sinh(\sqrt{\gamma}T)\} \left(v_0 + \frac{\hbar k}{2M}\right) + \\
&\quad \sqrt{\gamma}\{1 + \cosh[\sqrt{\gamma}(T + T')] - \\
&\quad 2\cosh(\sqrt{\gamma}T)\} \left(z_0 - \frac{g}{\gamma}\right) \Bigg), \tag{63}
\end{aligned}$$

which, to first order in γ and for $T = T'$ reduces to

$$kgT^2 + k\gamma T^2 \left[\frac{7}{12}gT^2 - (v_0 + \frac{\hbar k}{2M})T - z_0\right], \tag{64}$$

where the first term, which is precisely expression (61), gives huge phase shifts for matter-waves compared with

---

7. This Sagnac phase shift (in units of 2π) can be written as the projection of the orbital angular momentum (in units of $\hbar$) of the interfering particles. An example of nuclear Sagnac interferometer is provided by rotating molecules, for which this phase shift is naturally quantized.
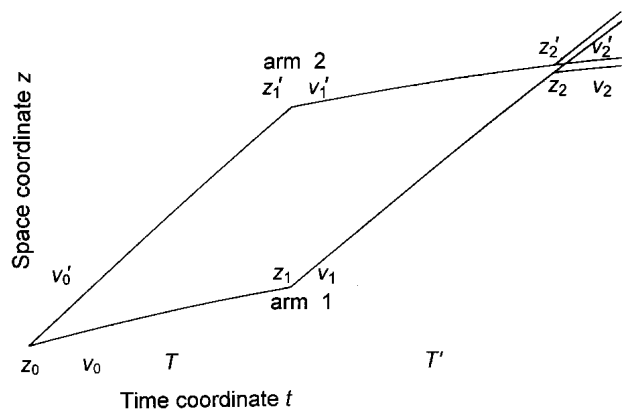
**Figure 18.** Space-time diagram of the atomic gravimeter.

what could be obtained with light rays, since the times T can be of the order of $1s$ and gT^2 is of the order of 10 m compared with an optical wavelength. The next term is a significant correction due to the gravitational field gradient γ. One can also measure directly these field gradients, with two gravimeters using two clouds of cold atoms and sharing the same vertical laser beam splitters. It is then no longer necessary to have a very sophisticated inertial platform for the reference mirror and it is possible to measure directly the differential acceleration between these two clouds. This is the principle, illustrated in Figure 19, of the gradiometers

developed first in Stanford then in Yale by Kasevich and co-workers [27, 59]. The current sensitivity is 4×10^{-9} s^{-2}/$\sqrt{\text{Hz}}$ and the uncertainty is 1×10^{-9} s^{-2}/$\sqrt{\text{Hz}}$ for an extrapolated 10 m separation between accelerometers. For the future, this principle may be considered for gravitational wave detection in space [60].

The first demonstration of a gyro using atom waves was performed at the Physikalisch-Technische Bundesanstalt in Braunschweig, Germany, in a joint collaboration with the present author [61] (Figure 20). The simplified first-order Sagnac phase shift formula (62) given above reveals the considerable gain in sensitivity brought by matter-waves, as, in this formula, the rest mass energy Mc^2 has to be replaced by the photon energy $h\nu$ in the case of light waves. This expression can be derived by a number of approaches, the best of which is to use the rotation operator in the Schrödinger equation and the derived propagator and $ABCD$ matrices, as outlined above, which gives the Sagnac shift thanks to an exact formula. The same approach applies to the trapezoid geometry used in the previous experiment as well as to the parallelogram geometry, as suggested in [24], analogue of the Mach-Zehnder optical interferometer, which has been used in more recent experiments and which has the advantage of being insensitive to laser detuning. For the illustration, the formula calculated with the $ABCD\xi$ formalism is
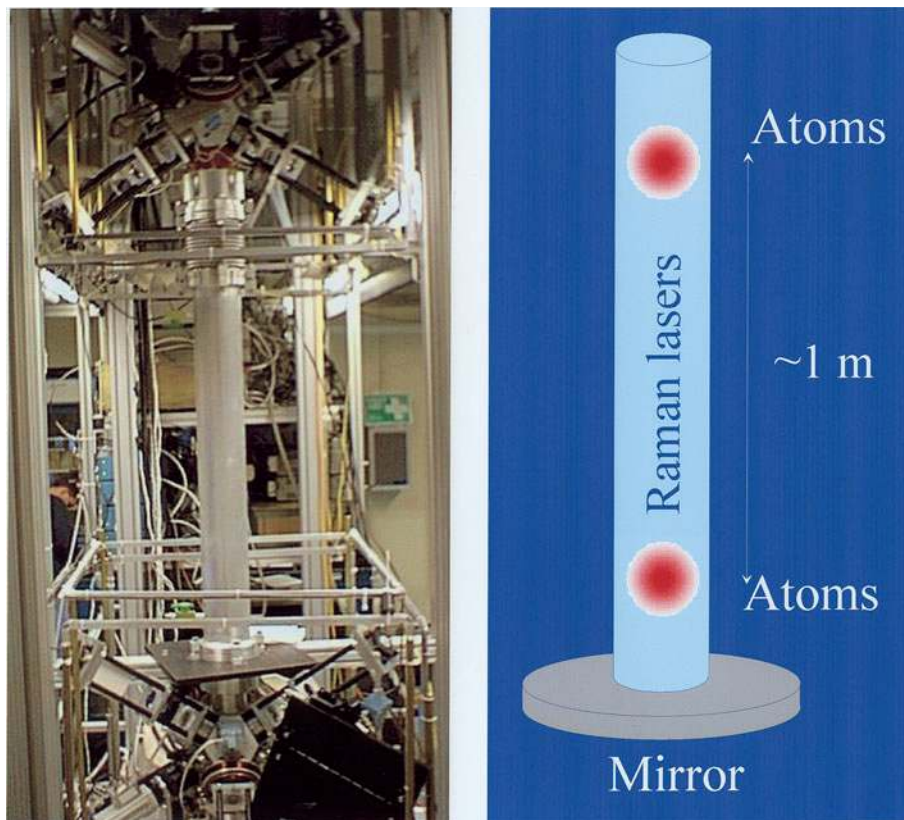
Figure 19. Atom wave gradiometer of Yale University. The two clouds of atoms share the same Raman beams, which generate two atom interferometers separated vertically by 1 m.
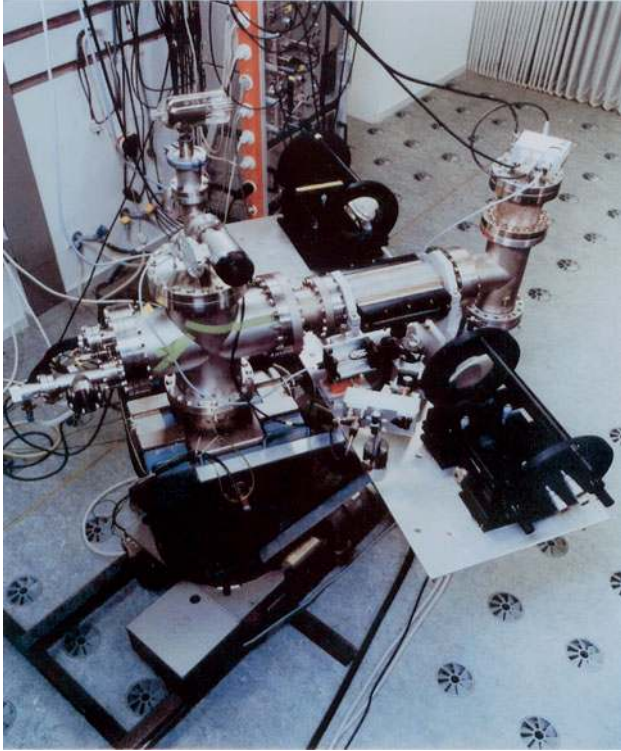
Figure 20. The first atom-wave gyro [61]. The calcium atomic beam originating from the oven on the left crosses two counterpropagating pairs of copropagating laser beams generated by the pair of cat's-eyes facing each other on the right platform. These four beams act as beam splitters, deflectors and recombiner for the atom waves and the excited state output of the interferometer is monitored via the fluorescence light by the photomultiplier on the extreme right of the apparatus. The whole set-up is mounted on a rotating table.
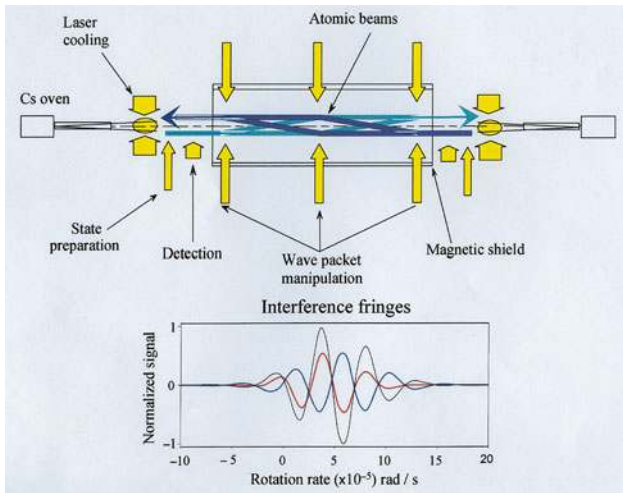
Figure 21. Atomic gyro developed at Yale in the group of Mark Kasevich. The Sagnac phases corresponding to the two opposite thermal atom beams have opposite signs and are subtracted. The Earth rotation is responsible for the offset.

in that case (with $T = T'$ and $\vec{k}_\perp = \vec{k} - \left(\vec{k} \cdot \hat{n}\right)\hat{n}$):[8]

$$
\begin{aligned}
\delta\varphi_{Sagnac} = {} & \sin(2\Omega T)\hat{n} \cdot \left[\vec{k} \times \vec{v}_0 T\right] + \\
& [\sin(2\Omega T) - 2\sin(\Omega T)]\hat{n} \\
& \cdot \left[\vec{k} \times (\vec{r}_0 + \vec{v}_0 T)\right] + \\
& \cos(2\Omega T)\left[\vec{k}_\perp \cdot (\vec{v}_0 + \frac{\hbar\vec{k}}{2M})T\right] + \vec{k}_\perp \cdot \vec{r}_0 + \\
& [\cos(2\Omega T) - 2\cos(\Omega T)] \\
& \left\{\vec{k}_\perp \cdot \left[\vec{r}_0 + (\vec{v}_0 + \frac{\hbar\vec{k}}{2M})T\right]\right\},
\end{aligned}
\tag{66}
$$

which simplifies if the Bragg condition $\vec{k}_\perp \cdot (\vec{p}_0 + \hbar\vec{k}/2) = 0$ is satisfied ($\vec{v}_0 = \vec{p}_0/M$ in the non-rotating frame). This formula does not include the corrections associated with the anomalous group velocity of atoms within the beam splitters [41-43] (let us recall that, during the interaction, the atom trajectories are perpendicular to the laser beams in the case of zero detuning and when the Bragg condition is satisfied, as in the neutron interferometers).

For rotations, the best sensitivity achieved to date is 6×10^{-10} rad s^{-1} Hz$^{-1/2}$ [62] with the set-up of Figure 21. Clearly, if the atomic motion is reversed h_{00} is unchanged, while $\vec{h} \cdot \vec{p}$ is reversed. This property is used to separate rotations and accelerations by means of counterpropagating atomic beams. A compact device (30 cm height) using cold atoms and the caesium clock technology (PHARAO) is under development in Paris, in a joint collaboration between several laboratories [63], and is shown in Figures 22 and 23. Here again, cold atoms are launched along counterpropagating parabolic trajectories, in order to separate the various components of the acceleration and of the rotation fields.

The sensitivity numbers quoted here are expected to improve rapidly in the near future, especially in

---

8. As in the gravitational field case considered above and treated in detail in [16], the symmetry of the interferometer is such that the action integral in the absence of perturbation is the same on both arms and does not make any contribution to the phase shift. In the presence of the gravito-inertial field the difference in action is exactly compensated by the phase difference on both paths before the last interaction, which comes from the separation of the end points and is easily evaluated at the mid-point (see Appendix 3). The Sagnac phase is then given by a simple sum over beam-splitter phase contributions $\vec{k} \cdot \vec{r} = \tilde{q}_{j0} k_{j0}$:

$$
-\sum_j \tilde{q}_{j0}\left[\exp\left(-i\hat{n} \cdot \vec{J}\,\theta_j\right) - 1\right]k_j,
\tag{65}
$$

in which the coordinates $\tilde{q}_{j0}$ are those of the successive positions of the interaction points in the inertial frame of the atoms. After the last interaction, a small additional contribution, of the order $\hbar k^2$, is associated with the laser phase difference between the two end points.
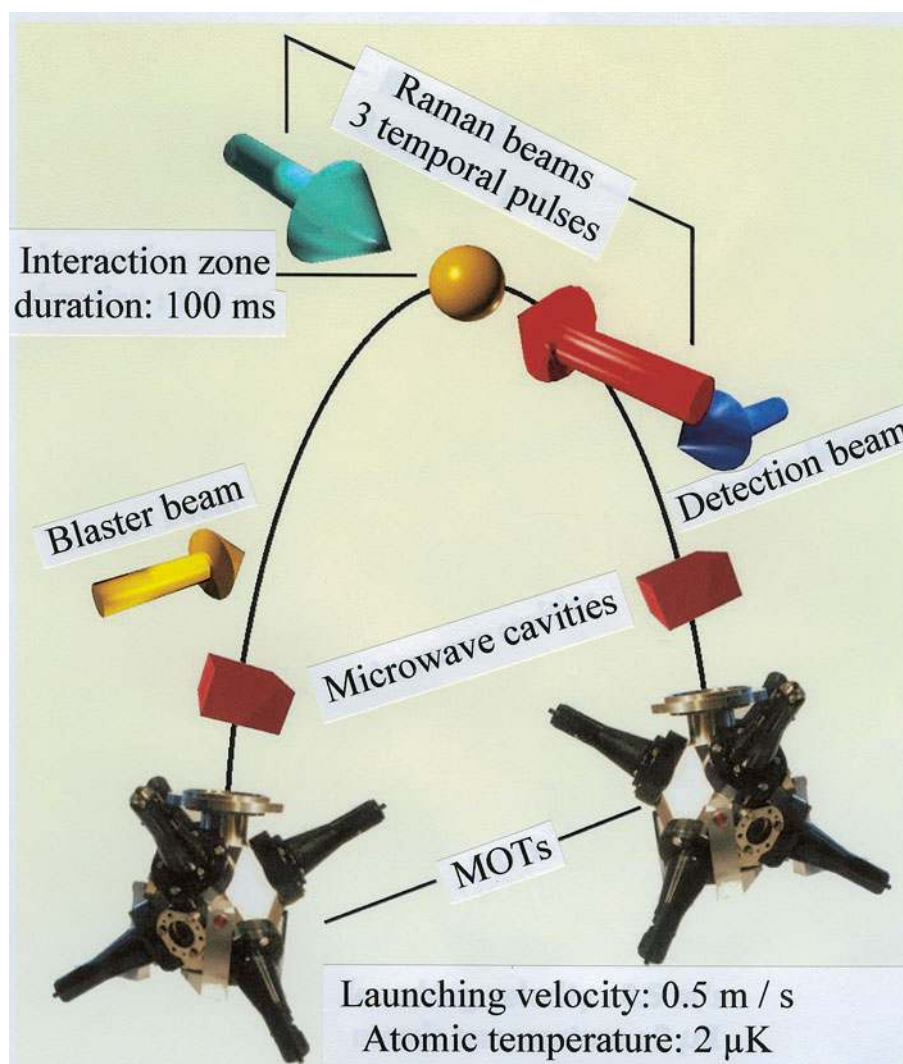
Figure 22. Principle of the cold caesium gyro-accelerometer developed at the Paris Observatory in collaboration between D. Holleville, J. Fils, A. Landragin, N. Dimarcq, A. Clairon (LHA and BNM-LPTF), Ph. Bouyer (IOTA), Ch. Salomon (LKB) and Ch. Bordé (LPL-ERGA).

space experiments, in which general relativistic effects should become detectable. The space project called HYPER [64] aims precisely at the detection of such effects thanks to the possibility of long drift times in space (Figure 24). This will considerably increase the sensivity of these devices. The technology of trapping and manipulating cold atoms developed for the project ACES (Atomic Clock Ensemble in Space) will be directly applicable to inertial sensors for many applications in deep space navigation of space probes. Among the goals of HYPER, there is a very accurate measurement of the fine structure constant α, a test of the equivalence principle at the atomic level, using two different atomic species in the interferometer, a detection of the periodic signal from the latitudinal dependence of the Lense-Thirring effect in polar orbit, decoherence studies ... . In fact, atom interferometers are so sensitive to gravito-inertial fields and to their gradients that it will be necessary during the next few years to develop many new techniques and tricks in the field of atom optics (e.g. phase conjugation of atom waves) to isolate the specific signature of investigated phenomena.

An accurate measurement of the effect of gravitation and inertia on antimatter also appears as a possibility already discussed in [65] with a transmission-grating interferometer, although we believe, for obvious reasons, that an antiatom interferometer using laser beams for the antihydrogen beam splitters (so-called Ramsey-Bordé interferometers) would be better suited for such an experiment. Such an interferometer has been recently demonstrated for hydrogen [35]. Coherent beams of antihydrogen will be produced either by Bose-Einstein condensation and/or by stimulated bosonic amplification[9] [7].

---

9. Using for example a reaction such as antiproton + positronium $\rightarrow$ antihydrogen + electron.
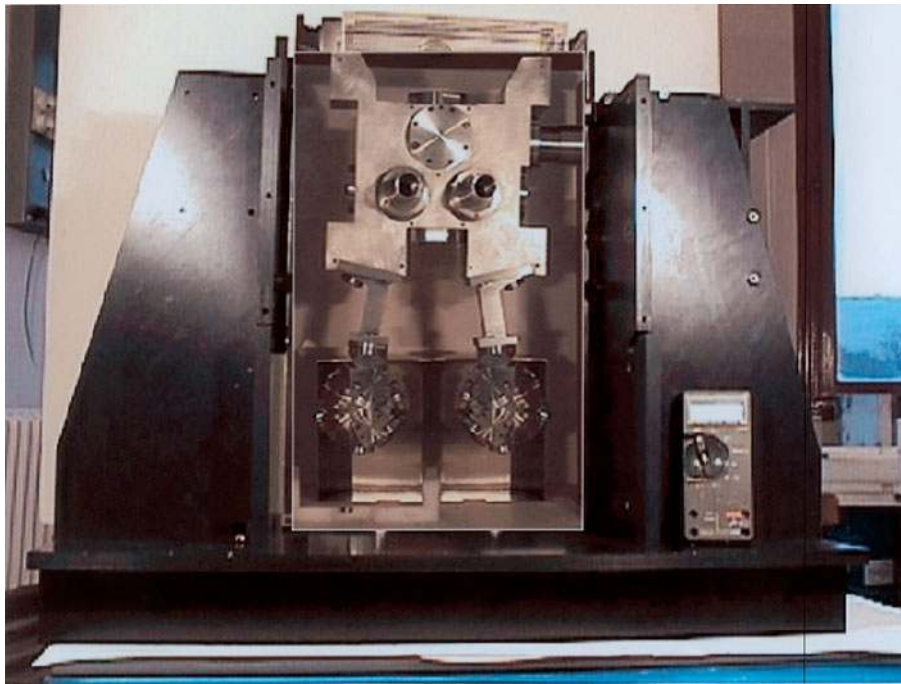
Figure 23. Cold-atom gyro-accelerometer under construction at the Paris Observatory.
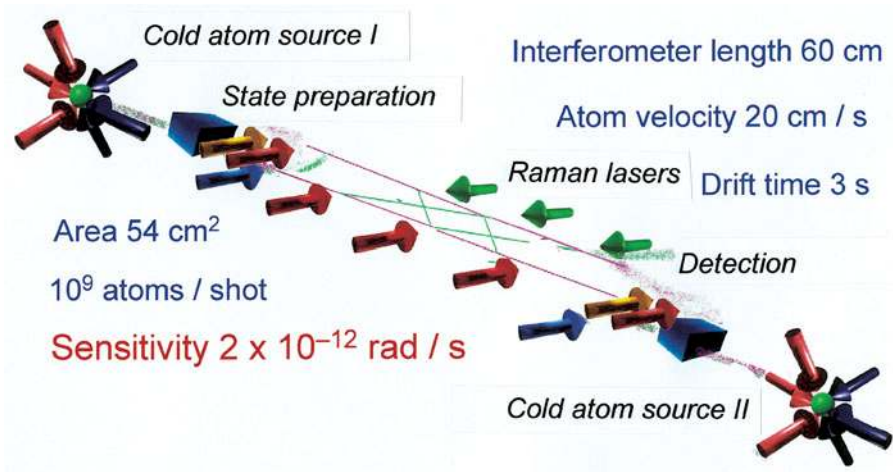

Figure 24. Schematic of an atom interferometer in space providing long drift times and a large interferometer area.

Appendix 1

Stationary fountain solution

In this appendix, we show how the well-known stationary solution of the Schrödinger equation for atoms in the presence of a constant gravitational field [19, 20] can be adapted to the fountain clock problem. The vertical gravitational potential for atoms in the internal energy state α is $M_\alpha g x$, where x is the vertical coordinate. If the constant energy of the atoms is E, the time-independent Schrödinger equation reads

$$\nabla^2 \Psi + \frac{2M_\alpha}{\hbar^2}(E - M_\alpha g x)\Psi = 0. \tag{67}$$

If we introduce the dimensionless coordinates

$$\xi = \frac{1}{l}\left(\frac{E}{M_\alpha g} - x\right), \eta = \frac{y}{l}, \zeta = \frac{z}{l}, \tag{68}$$

thanks to the length

$$l = \left(\frac{\hbar^2}{2M_\alpha^2 g}\right)^{1/3}, \tag{69}$$

the Schrödinger equation can be rewritten in a form free of parameters:

$$\left[\frac{\partial^2}{\partial \xi^2} + \frac{\partial^2}{\partial \eta^2} + \frac{\partial^2}{\partial \zeta^2} + \xi\right]\Psi = 0. \tag{70}$$

We seek a solution of the form

$$\Psi(\xi, \eta, \zeta) = \psi(\xi)\varphi(\xi, \eta, \zeta), \tag{71}$$

in which $\varphi(\xi, \eta, \zeta)$ carries the transverse dependence in η, ζ and is a slowly varying function of ξ. These functions satisfy

$$\left[\frac{\partial^2}{\partial \xi^2} + \xi\right]\psi = 0 \tag{72}$$

$$\frac{\partial^2 \varphi}{\partial \eta^2} + \frac{\partial^2 \varphi}{\partial \zeta^2} + \frac{2}{\psi}\frac{\partial \psi}{\partial \xi}\frac{\partial \varphi}{\partial \xi} = 0, \tag{73}$$

where $\partial^2 \varphi/\partial \xi^2$ has been neglected in the second equation. The first equation has the well-known Airy solutions[10]

$$\psi^{\pm}(\xi) = \frac{1}{2}[\mathrm{Ai}(-\xi) \pm i\mathrm{Bi}(-\xi)]. \tag{74}$$

Most useful for our purpose is the asymptotic expression of these Airy functions:

$$\mathrm{Ai}(-\xi) \pm i\mathrm{Bi}(-\xi) \overset{\xi \to +\infty}{\longrightarrow} \frac{1}{\sqrt{\pi}\xi^{1/4}}$$
$$\exp\left[\mp i\left(\frac{2}{3}\xi^{3/2} - \frac{\pi}{4}\right)\right]. \tag{75}$$

From this solution, we may approximate $(2/\psi)\partial\psi/\partial\xi$ by $\pm 2i\xi^{1/2}$ and replace the second equation by

$$\frac{\partial^2 \varphi^{\pm}}{\partial \eta^2} + \frac{\partial^2 \varphi^{\pm}}{\partial \zeta^2} \mp 2i\xi^{1/2}\frac{\partial \varphi^{\pm}}{\partial \xi} = 0, \tag{76}$$

which, by shifting to the new variable

$$\tau = \int_0^{\xi}\frac{\mathrm{d}\xi'}{\xi'^{1/2}} = 2\xi^{1/2}, \tag{77}$$

becomes

$$\frac{\partial^2 \varphi^{\pm}}{\partial \eta^2} + \frac{\partial^2 \varphi^{\pm}}{\partial \zeta^2} \mp 2i\frac{\partial \varphi^{\pm}}{\partial \tau} = 0. \tag{78}$$

The functions $\varphi^{\pm}$ are thus given by the usual counterpropagating solutions $U^{\pm*}$ of laser mode theory in free space [10] with $k = 1$, i.e. by expressions easily obtained from (7), (8) and (9) of the main text. We write the general solution as

$$\Psi(\tau, \eta, \zeta) = \psi^+(\tau)\varphi^+(\tau, \eta, \zeta) + \psi^-(\tau)\varphi^-(\tau, \eta, \zeta), \tag{79}$$

where, as Ψ depends on x only through ξ, the wave propagating downwards $\psi^-(\xi)\varphi^-(\tau, \eta, \zeta)$ is obtained from the upward solution $\psi^+(\xi)\varphi^+(\tau, \eta, \zeta)$ by reflection from the horizontal plane $\xi = 0$. A special case, which satisfies reversal symmetry, is $\varphi^- = \varphi^{+*}$ with a waist at $\xi = 0$.

10. This solution is not normalized. The normalization constant is $1/(l\sqrt{Mg})$, see [19].

A better way to obtain exact solutions and to reach the same conclusions is to look for transversally plane wave solutions of (67):

$$\Psi_{\vec{p}_{\perp}} = e^{i\vec{p}_{\perp}\cdot\vec{r}_{\perp}/\hbar}\psi(\xi'), \tag{80}$$

where $\psi(\xi')$ satisfies

$$\left(\frac{\partial^2}{\partial \xi'^2} + \xi'\right)\psi(\xi') = 0 \tag{81}$$

with, this time,

$$\xi' = \frac{1}{l}\left(\frac{E - E_{\perp}}{M_{\alpha}g} - x\right) = \xi - \frac{E_{\perp}}{M_{\alpha}gl} \tag{82}$$

and

$$E_{\perp} = p_{\perp}^2/2M_{\alpha} = \hbar^2 k_{\perp}^2/2M_{\alpha}. \tag{83}$$

The general exact solution is therefore

$$\Psi(\vec{r}_{\perp}, \xi) = \frac{1}{2\pi\hbar}\int \mathrm{d}^2 p_{\perp}a(\vec{p}_{\perp})$$
$$e^{i\vec{p}_{\perp}\cdot\vec{r}_{\perp}/\hbar}\mathrm{Ai}\big(-(\xi - p_{\perp}^2 l^2/\hbar^2)\big), \tag{84}$$

which we can split into upgoing and downgoing solutions with (74). If $a(\vec{p}_{\perp})$ is real, $\Psi(\vec{r}_{\perp}, \xi)$ is real and satisfies time-reversal symmetry.

If we use cylindrical coordinates, this solution can be written

$$\Psi(r_{\perp}, \phi, \xi) = \frac{1}{2\pi\hbar}\int_0^{2\pi}\mathrm{d}\beta\int_0^{+\infty}p_{\perp}\mathrm{d}p_{\perp}a(p_{\perp}, \beta)$$
$$e^{ip_{\perp}r_{\perp}\cos(\phi-\beta)/\hbar}\mathrm{Ai}\big(-(\xi - p_{\perp}^2 l^2/\hbar^2)\big), \tag{85}$$

which can be expanded into a Fourier series of the azimuthal angle β of $\vec{p}_{\perp}$ as in [10]. By way of illustration, if we have a fountain with cylindrical symmetry, we can use

$$\frac{1}{2\pi}\int_0^{2\pi}\mathrm{d}\beta e^{ik_{\perp}r_{\perp}\cos(\phi-\beta)} = J_0(k_{\perp}r_{\perp}) \tag{86}$$

to write the solution as a single integral (the factor $1/\hbar$ is omitted):

$$\Psi(r_{\perp}, \xi) = \int_0^{+\infty}k_{\perp}\mathrm{d}k_{\perp}a(k_{\perp})$$
$$J_0(k_{\perp}r_{\perp})\mathrm{Ai}\big[-(\xi - k_{\perp}^2 l^2)\big], \tag{87}$$

and finally, for a Gaussian spectrum of $k_{\perp}$ (with a phase written in a way that will become clear below):

$$\Psi(r_{\perp}, \xi) = \frac{1}{\Delta^2}\int_0^{+\infty}k_{\perp}\mathrm{d}k_{\perp}$$
$$\exp\left[-\frac{k_{\perp}^2}{2\Delta^2}\big(1 + i\Delta^2 l^2 \tau_0\big)\right]$$
$$J_0(k_{\perp}r_{\perp})\mathrm{Ai}\big[-(\xi - k_{\perp}^2 l^2)\big], \tag{88}$$

which we can again split into upgoing and downgoing solutions with (74), which is easily calculated with a program such as Mathematica and has indeed been used by the author to investigate the amplitude and wave-front structure of this solution.

The general solution has the asymptotic form

$$\Psi(\vec{r}_\perp, \xi) = \frac{1}{2\pi\hbar} \frac{1}{2\sqrt{\pi}\xi^{1/4}} \int d^2 p_\perp a(\vec{p}_\perp) e^{i\vec{p}_\perp \cdot \vec{r}_\perp/\hbar}$$
$$\left(\exp\left\{ -i\left[\frac{2}{3}(\xi - p_\perp^2 l^2/\hbar^2)^{3/2} - \frac{\pi}{4} \right] \right\} + \right.$$
$$\left. \exp\left\{ i\left[\frac{2}{3}(\xi - p_\perp^2 l^2/\hbar^2)^{3/2} - \frac{\pi}{4} \right] \right\} \right), \quad (89)$$

where $\xi'^{1/4}$ has been approximated by $\xi^{1/4}$ in the denominator, as $p_\perp^2 l^2/\hbar^2 \ll \xi$ far from the fountain apex. For the same reason, we may expand the phase

$$\Psi(\vec{r}_\perp, \xi) = \frac{1}{2\pi\hbar} \frac{1}{2\sqrt{\pi}\xi^{1/4}}$$
$$\left\{ \exp\left[-i\left(\frac{2}{3}\xi^{3/2} - \frac{\pi}{4} \right) \right] \int d^2 p_\perp a(\vec{p}_\perp) \right.$$
$$e^{i\vec{p}_\perp \cdot \vec{r}_\perp/\hbar} \exp\left(ip_\perp^2 l^2 \xi^{1/2}/\hbar^2 \right) +$$
$$\exp\left[i\left(\frac{2}{3}\xi^{3/2} - \frac{\pi}{4} \right) \right] \int d^2 p_\perp a(\vec{p}_\perp)$$
$$\left. e^{i\vec{p}_\perp \cdot \vec{r}_\perp/\hbar} \exp\left(-ip_\perp^2 l^2 \xi^{1/2}/\hbar^2 \right) \right\}. \quad (90)$$

We recover the form

$$\Psi(\tau, \eta, \zeta) = \psi^+(\tau)\varphi^+(\tau, \eta, \zeta) + \psi^-(\tau)\varphi^-(\tau, \eta, \zeta) \quad (91)$$

with an explicit expression of the solution

$$\varphi^\pm(\tau, \eta, \zeta) = \frac{1}{2\pi\hbar} \int d^2 p_\perp a(\vec{p}_\perp) e^{i\vec{p}_\perp \cdot \vec{r}_\perp/\hbar}$$
$$\exp\left(\pm ip_\perp^2 l^2 \tau/2\hbar^2 \right), \quad (92)$$

which obviously satisfies (78) and where $a(\vec{p}_\perp)$ can be expanded in Hermite-Gauss, Laguerre-Gauss ... functions. If the wave is plane (waist) in the horizontal plane $\tau = \tau_0$ for the ascending wave and $\tau = -\tau_0$ for the descending wave (as τ is positive in the physically accessible region, only one of these possibilities will occur, depending on the sign of τ_0):

$$\varphi^\pm(\tau, \eta, \zeta) = \frac{1}{2\pi\hbar} \int d^2 p_\perp |a(\vec{p}_\perp)| e^{i\vec{p}_\perp \cdot \vec{r}_\perp/\hbar}$$
$$\exp\left[\pm ip_\perp^2 l^2 (\tau \pm \tau_0)/2\hbar^2 \right], \quad (93)$$

and if $\tau_0 = 0$ the upward and downward waves have matched wave-fronts: $\varphi^- = \varphi^{+*}$. In the simple case of

the Gaussian spectrum of $k_\perp$ (see [11], Appendix B):

$$\varphi^\pm(\tau, \eta, \zeta) = \frac{1}{2\pi\Delta^2} \int d^2 k_\perp \exp\left(-\frac{k_\perp^2}{2\Delta^2} - ik_\perp^2 l^2 \tau_0/2 \right)$$
$$e^{i\vec{k}_\perp \cdot \vec{r}_\perp/\hbar} \exp\left(\pm ik_\perp^2 l^2 \tau/2 \right)$$
$$= L^\pm \exp\left(-L^\pm \Delta^2 \frac{r_\perp^2}{2} \right), \quad (94)$$

with

$$L^\pm = \frac{1}{1 \mp i\Delta^2 l^2 (\tau \mp \tau_0)}. \quad (95)$$

Apart from wave-front considerations, the phase difference between the downward and upward waves is

$$\Phi = \frac{4}{3}\xi^{3/2} = \frac{4}{3}\left(\frac{2M_\alpha^2 g}{\hbar^2} \right)^{1/2} \left(\frac{E}{M_\alpha g} - x \right)^{3/2}. \quad (96)$$

To investigate how this phase changes with the various parameters, let us calculate its partial derivatives, at the return point $x = x_0$, where the atoms recover their initial velocity v_0:

$$\left(\frac{\partial \Phi}{\partial E} \right)_{x=x_0} = \frac{2\sqrt{2(E - M_\alpha g x_0)}}{\hbar g} = \frac{2v_0}{\hbar g}; \quad (97)$$

$$\left(\frac{\partial \Phi}{\partial k_x} \right)_{x=x_0} = \left(\frac{\partial \Phi}{\partial E} \right)_{x=x_0} \frac{\partial E}{\partial k_x}$$
$$= \left(\frac{\partial \Phi}{\partial E} \right)_{x=x_0} \frac{\hbar^2 k_x}{M_\alpha} = \frac{2v_0^2}{g}; \quad (98)$$

$$\left(\frac{\partial \Phi}{\partial M} \right)_{x=x_0} = -\frac{1}{3}\frac{v_0^3}{\hbar g}. \quad (99)$$

Hence the phase associated with the detuning $\delta k_x = [\omega - \omega_{ba}(v) \mp kv_z - \delta]/v_x$ is

$$\left(\frac{\partial \Phi}{\partial k_x} \right)_{x=x_0} \delta k_x = \frac{2v_0^2}{g}\delta k_x, \quad (100)$$

and the phase associated with the second-order Doppler shift combined with the gravitational shift is

$$\left(\frac{\partial \Phi}{\partial M} \right)_{x=x_0} (E_b - E_a)/c^2 = -\omega_{ba}\frac{1}{6}\frac{v_0^2}{c^2}\frac{2v_0}{g}. \quad (101)$$

Appendix 2

Derivation of the quantum-mechanical propagator for atom waves in the presence of gravito-inertial fields and general solution of Schrödinger equation

We start with the following equation obtained in the main text for the state vector in the "non-rotating"

frame:

$$i\hbar\frac{\partial|\Psi_0(t)\rangle}{\partial t} = \left[H_0 + \frac{1}{2M}\overrightarrow{p}_{op}\cdot\overrightarrow{g_0}(t)\cdot\overrightarrow{p}_{op} - M\overrightarrow{g_0}(t)\cdot\vec{r}_{op} - \frac{M}{2}\vec{r}_{op}\cdot\overrightarrow{\gamma_0}(t)\cdot\vec{r}_{op} + V_0(\vec{r}_{op},t)\right]$$
$$|\Psi_0(t)\rangle. \tag{102}$$

For simplicity, in the following, we omit the subscript 0 for the "non-rotating" frame. We denote by $\overrightarrow{n}(t)$ the tensor such that $n^{ij}g_{kl}=\delta^j_k$, and by n^{-1}, γ, g, Ω the matrices corresponding to the tensors $\overrightarrow{g}(t)$, $\overrightarrow{\gamma}(t)$ and vectors $\vec{g}(t)$, $\overrightarrow{\Omega}(t)$. Owing to the hermiticity of the Hamiltonian, n^{-1}, γ and g are real symmetric matrices.

As shown in detail in [10] in the one-dimensional case, a new series of unitary transformations,

$$|\widetilde{\Psi}(t)\rangle = U^{-1}|\Psi_0(t)\rangle, \tag{103}$$

where

$$U(t,t') = U_1(t,t') \ldots U_6(t,t')\exp\left[-iH_0(t-t')/\hbar\right] \tag{104}$$

eliminates one term after the other and brings (31) to the form

$$i\hbar\frac{\partial|\widetilde{\Psi}(t)\rangle}{\partial t} = \widetilde{V}(\vec{r}_{op},\overrightarrow{p}_{op},t)|\widetilde{\Psi}(t)\rangle. \tag{105}$$

The first transformation

$$U_1 = \exp\left[-\frac{i}{\hbar}\vec{\xi}(t)\cdot\vec{p}_{op}\right] \tag{106}$$

is a space translation, which gives the new equation

$$i\hbar\frac{\partial|\Psi_1(t)\rangle}{\partial t} = \left[H_0 + \frac{1}{2M}\overrightarrow{p}_{op}\cdot\overrightarrow{g}(t)\cdot\overrightarrow{p}_{op} - M\overrightarrow{g}(t)\cdot(\vec{r}_{op}+\vec{\xi}) - \overrightarrow{\dot{\xi}}\cdot\overrightarrow{p}_{op} - \frac{M}{2}(\vec{r}_{op}+\vec{\xi})\cdot\overrightarrow{\gamma}(t)\cdot(\vec{r}_{op}+\vec{\xi}) + V((\vec{r}_{op}+\vec{\xi}),t)\right]|\Psi_1(t)\rangle. \tag{107}$$

Then

$$U_2 = \exp\left[\frac{iM}{\hbar}\overrightarrow{\dot{\xi}}\cdot\overrightarrow{n}(t)\cdot\vec{r}_{op}\right] \tag{108}$$

is a boost, which yields

$$i\hbar\frac{\partial|\Psi_2(t)\rangle}{\partial t} = \left[H_0 + \frac{1}{2M}\left(\overrightarrow{p}_{op}+M\overrightarrow{\dot{\xi}}\cdot\overrightarrow{n}\right)\cdot\overrightarrow{g}(t)\cdot\left(\overrightarrow{p}_{op}+M\overrightarrow{\dot{\xi}}\cdot\overrightarrow{n}\right) - M\overrightarrow{g}\cdot(\vec{r}_{op}+\vec{\xi}) - \overrightarrow{\dot{\xi}}\cdot\left(\overrightarrow{p}_{op}+M\overrightarrow{\dot{\xi}}\cdot\overrightarrow{n}\right) + M\overrightarrow{\ddot{\xi}}\cdot\overrightarrow{n}\cdot\vec{r}_{op} + M\overrightarrow{\dot{\xi}}\cdot\overrightarrow{\dot{n}}\cdot\vec{r}_{op} - \frac{M}{2}(\vec{r}_{op}+\vec{\xi})\cdot\overrightarrow{\gamma}(t)\cdot(\vec{r}_{op}+\vec{\xi}) + V((\vec{r}_{op}+\vec{\xi}),t)\right]|\Psi_2(t)\rangle. \tag{109}$$

Thirdly,

$$U_3 = \exp\left[\frac{i}{\hbar}\int_{t'}^t L(t_1)\mathrm{d}t_1\right] \tag{110}$$

is a gauge transformation and the equation for

$$|\Psi_3(t)\rangle = U_3^{-1}U_2^{-1}U_1^{-1}|\Psi(t)\rangle \tag{111}$$

reads

$$i\hbar\frac{\partial|\Psi_3(t)\rangle}{\partial t} = \left[H_0 + \frac{1}{2M}\overrightarrow{p}_{op}\cdot\overrightarrow{g}(t)\cdot\overrightarrow{p}_{op} - \frac{M}{2}\vec{r}_{op}\cdot\overrightarrow{\gamma}(t)\cdot\vec{r}_{op} + V((\vec{r}_{op}+\vec{\xi}),t)\right]|\Psi_3(t)\rangle. \tag{112}$$

Then we apply successively[11]

$$U_4 = \exp\left[i\vec{r}_{op}\cdot\overrightarrow{\lambda}(t)\cdot\vec{r}_{op}\right], \tag{113}$$

where $\overrightarrow{\lambda}(t)$ satisfies

$$\frac{\mathrm{d}\overrightarrow{\lambda}}{\mathrm{d}t} = \frac{M\overrightarrow{\gamma}}{2\hbar} - \frac{2\hbar}{M}\overrightarrow{\lambda}\cdot\overrightarrow{g}\cdot\overrightarrow{\lambda} \tag{114}$$

and

$$U_5 = \exp\left[i\overrightarrow{p}_{op}\cdot\overrightarrow{\mu}(t)\cdot\overrightarrow{p}_{op}/\hbar^2\right] \tag{115}$$

where $\overrightarrow{\mu}(t)$ satisfies

$$\frac{\mathrm{d}\overrightarrow{\mu}}{\mathrm{d}t} = -\frac{\hbar\overrightarrow{g}}{2M} + \frac{2\hbar}{M}\left(\overrightarrow{g}\cdot\overrightarrow{\lambda}\cdot\overrightarrow{\mu}+\overrightarrow{\mu}\cdot\overrightarrow{\lambda}\cdot\overrightarrow{g}\right), \tag{116}$$

so that

$$i\hbar\frac{\partial|\Psi_5(t)\rangle}{\partial t} = \left\{H_0 + \frac{\hbar}{M}[\overrightarrow{r}_{op}\cdot\overrightarrow{\lambda}\cdot\overrightarrow{g}\cdot\overrightarrow{p}_{op} + \overrightarrow{p}_{op}\cdot\overrightarrow{g}\cdot\overrightarrow{\lambda}(t)\cdot\overrightarrow{r}_{op}] + V(\vec{r}_{op}-2\overrightarrow{\mu}(t)\cdot\overrightarrow{p}_{op}/\hbar+\vec{\xi},t)\right\}|\Psi_5(t)\rangle; \tag{117}$$

and finally

$$U_6 = \mathcal{T}\exp\left[-\frac{i}{M}\int_{t'}^t \mathrm{d}t_1\left(\overrightarrow{r}_{op}\cdot\overrightarrow{\lambda}\cdot\overrightarrow{g}\cdot\overrightarrow{p}_{op} + \overrightarrow{p}_{op}\cdot\overrightarrow{g}\cdot\overrightarrow{\lambda}\cdot\overrightarrow{r}_{op}\right)\right]$$
$$= \mathcal{T}\exp\left[-\frac{2i}{M}\int_{t'}^t \mathrm{d}t_1\left(\overrightarrow{r}_{op}\cdot\overrightarrow{\lambda}\cdot\overrightarrow{g}\cdot\overrightarrow{p}_{op}\right)\right]$$
$$\exp\left(-\frac{\hbar}{M}Tr\int_{t'}^t\overrightarrow{\lambda}\cdot\overrightarrow{g}\,\mathrm{d}t_1\right) \tag{118}$$

("affinity operator" analogous to the rotation operator).

---

11. For all these calculations, we use the operator identity
$e^{\xi A}Be^{-\xi A} = B + \xi[A,B] + \frac{\xi^2}{2!}[A,[A,B]] + \ldots$.

$$i\hbar\frac{\partial \mid \Psi_6(t) >}{\partial t} = \left\{ H_0 + V(U_6^{-1}(\vec{r}_{op} - 2\overset{\Rightarrow}{\vec{\mu}}(t) \right.$$
$$\left. \cdot \vec{p}_{op}/\hbar + \vec{\xi})U_6, t) \right\} \mid \Psi_6(t) >$$
$$= \left\{ H_0 + V(\vec{R}_{op}(t), t) \right\} \mid \Psi_6(t) > \tag{119}$$

with

$$\vec{R}_{op}(t) = A \cdot \vec{r}_{op} + B \cdot \vec{p}_{op}/M + \vec{\xi}, \tag{120}$$

where the matrices A and B are introduced below. The free propagator (in the absence of V) is therefore

$$\mathcal{K}_T(\vec{r}, \vec{r}', t, t')$$
$$= < \vec{r} \mid U(t, t') \mid \vec{r}' >$$
$$= \exp\left[-iH_0(t - t')/\hbar\right]$$
$$\quad < \vec{r} \mid U_1(t, t') \ldots U_6(t, t') \mid \vec{r}' >$$
$$= \exp\left[-iH_0(t - t')/\hbar\right]$$
$$\quad \exp\left\{ \frac{iM}{\hbar}\vec{\xi} \cdot \overset{\Rightarrow}{\vec{n}}(t) \cdot [\vec{r} - \vec{\xi}(t)] \right\}$$
$$\quad \exp\left[\frac{i}{\hbar}\int_{t'}^{t} L(t_1)dt_1\right]\mathcal{K}(\vec{r} - \vec{\xi}(t), \vec{r}', t, t'), \tag{121}$$

where

$$\mathcal{K}(\vec{r}, \vec{r}', t, t') = < \vec{r} \mid U_4(t, t')U_5(t, t')U_6(t, t') \mid \vec{r}' >. \tag{122}$$

From now on, we use a simple matrix notation for 3D vector and tensor components. The matrix elements of the operators are found to be

$$< \vec{r} \mid U_4(t, t') \mid \vec{r}' > = \exp\left[i\tilde{q}\lambda q\right] \tag{123}$$

$$< \vec{r} \mid U_5(t, t') \mid \vec{r}_1 > = \left(\frac{i}{4\pi}\right)^{3/2}\frac{1}{(\det \mu)^{1/2}}$$
$$\exp\left[-\frac{i}{4}(\tilde{q} - \tilde{q}_1)\mu^{-1}(q - q_1)\right] \tag{124}$$

$$< \vec{r}_1 \mid U_6(t, t') \mid \vec{r}' > = (\det A)^{1/2}\delta(q_1 - Aq'), \tag{125}$$

where the matrix A is given by

$$A = \mathcal{T}\exp\left[\frac{2\hbar}{M}\int_{t'}^{t} n^{-1}\lambda dt_1\right]. \tag{126}$$

We find

$$\mathcal{K}(q, q', t, t')$$
$$= \exp\left[i\tilde{q}\lambda q\right]\left(\frac{i}{4\pi}\right)^{3/2}\frac{(\det A)^{1/2}}{(\det \mu)^{1/2}}\int dq_1$$

$$\exp\left[-\frac{i}{4}(\tilde{q} - \tilde{q}_1)\mu^{-1}(q - q_1)\right]\delta(q_1 - Aq')$$
$$= \left(\frac{M}{2\pi i\hbar}\right)^{3/2}|\det B|^{-1/2}$$
$$\exp\left[\left(\frac{iM}{2\hbar}\right)(\tilde{q}DB^{-1}q - \right.$$
$$\left. 2\tilde{q}\widetilde{B^{-1}}q' + \tilde{q}'B^{-1}Aq')\right] \tag{127}$$

with the following relations:

$$\widetilde{B^{-1}} = -\frac{\hbar}{2M}\mu^{-1}A \tag{128}$$

$$C = \frac{2\hbar}{M}\lambda A \tag{129}$$

$$DB^{-1} = \frac{2\hbar}{M}\left(\lambda - \frac{1}{4}\mu^{-1}\right) \tag{130}$$

$$\widetilde{B^{-1}} = DB^{-1}A - C. \tag{131}$$

These matrices satisfy

$$\frac{d}{dt}\begin{pmatrix} A & B \\ C & D \end{pmatrix} = \begin{pmatrix} 0 & n^{-1} \\ \gamma & 0 \end{pmatrix}\begin{pmatrix} A & B \\ C & D \end{pmatrix}. \tag{132}$$

By construction, the propagator is a solution of the Schrödinger equation for any q'. We may therefore write a general solution, which has the same structure and a set of matrices of parameters X and Y that satisfy the same equations as the $ABCD$ matrices. We write this analogous matrix as

$$\begin{pmatrix} -\frac{i}{2}X^* & \frac{M}{2\hbar}X \\ -\frac{i}{2}Y^* & \frac{M}{2\hbar}Y \end{pmatrix}. \tag{133}$$

With this correspondence, this general solution is the generalized coherent state:

$$\mathcal{G}_\alpha(q, t) = N|\det X|^{-1/2}$$
$$\exp\left[\left(\frac{iM}{2\hbar}\right)\tilde{q}YX^{-1}q - 2i\tilde{q}\tilde{X}^{-1}\alpha + \frac{1}{2}\tilde{\alpha}X^{-1}X^*\alpha\right], \tag{134}$$

where N is a normalization constant. It is an eigenvector of the following annihilation operator (not to be confused with the matrix A introduced previously):

$$A = \left(\frac{M}{2\hbar}\right)\tilde{Y}q + \frac{i}{2}\tilde{X}\frac{d}{dq} \tag{135}$$

and plays the role of a generating function for 3D Hermite-Gauss solutions [9, 66]:

$$|\det X|^{-1/2}$$
$$\exp\left[\left(\frac{iM}{2\hbar}\right)\tilde{q}YX^{-1}q - 2i\tilde{q}\tilde{X}^{-1}\alpha + \frac{1}{2}\tilde{\alpha}X^{-1}X^*\alpha\right]$$

$$= |\det X|^{-1/2}$$

$$\exp\left[\left(\frac{iM}{2\hbar}\right)\tilde{q}YX^{-1}q\right]$$

$$\sum_{l,m,n} i^{l+m+n}\alpha_x^l\alpha_y^m\alpha_z^n\mathcal{H}_{lmn}(-2X^{-1}q;-X^{-1}X^*/2).$$

(136)

In order to determine the action of the propagator on any of these 3D Hermite-Gauss solutions, it will thus be sufficient to consider this action on a wave packet obtained from the generating function:

$$\int \mathrm{d}q'\mathcal{K}_T(q,q',t,t_0)\mathcal{G}_\alpha(q'-q_0,t_0)$$

$$\exp\left[i\tilde{p}_0(q'-q_0)/\hbar\right]$$

$$= \exp\left[-iE(t-t_0)/\hbar\right]\exp\left[\frac{iM}{\hbar}\widetilde{\xi}n(q-\xi)\right]$$

$$\exp\left[\frac{i}{\hbar}\int_{t_0}^t L(t_1)\mathrm{d}t_1\right]$$

$$\int \mathrm{d}q'\mathcal{K}(q-\xi,q',t,t_0)\mathcal{G}_\alpha(q'-q_0,t_0)$$

$$\exp\left[i\tilde{p}_0(q'-q_0)/\hbar\right],$$

(137)

which gives

$$\exp\left[-iE(t-t_0)/\hbar\right]\exp\left[\frac{iM}{\hbar}\widetilde{\xi}n(q-\xi)\right]$$

$$\exp\left[\frac{i}{\hbar}\int_{t_0}^t L(t_1)\mathrm{d}t_1\right]$$

$$\left(\frac{M}{2\pi i\hbar}\right)^{3/2}|\det B|^{-1/2}\int \mathrm{d}q'$$

$$\exp\left[\left(\frac{iM}{2\hbar}\right)\left[(\tilde{q}-\tilde{\xi})DB^{-1}(q-\xi)-\right.\right.$$

$$\left.\left. 2(\tilde{q}-\tilde{\xi})\widetilde{B^{-1}}q'+\tilde{q}'B^{-1}A q'\right]\right]$$

$$|\det X_0|^{-1/2}\exp\left[\left(\frac{iM}{2\hbar}\right)(\tilde{q}'-\tilde{q}_0)Y_0X_0^{-1}(q'-q_0)-\right.$$

$$\left. 2i(\tilde{q}'-\tilde{q}_0)\tilde{X}_0^{-1}\alpha+\frac{1}{2}\tilde{\alpha}X_0^{-1}X_0^*\alpha\right]$$

$$\exp\left[i\tilde{p}_0(q'-q_0)/\hbar\right]$$

$$= \exp\left[\frac{iS_{cl}(t,t_0)}{\hbar}\right]|\det X|^{-1/2}\exp\left[i\tilde{p}_1(q-q_1)/\hbar\right]$$

$$\exp\left[\left(\frac{iM}{2\hbar}\right)(\tilde{q}-\tilde{q}_1)YX^{-1}(q-q_1)-\right.$$

$$\left. 2i(\tilde{q}-\tilde{q}_1)\tilde{X}^{-1}\alpha+\frac{1}{2}\tilde{\alpha}X^{-1}X^*\alpha\right],$$

(138)

where $S_{cl}(t,t_0)$ is the classical action:

$$S_{cl}(t,t_0) = -E(t-t_0) + M\widetilde{\xi}nq_1 -$$

$$\frac{M}{2}\int_{t_0}^t (\widetilde{\xi}n\dot{\xi}+\widetilde{\xi}\gamma\xi)\mathrm{d}t_1 +$$

$$\frac{1}{2}(M\tilde{q}_0\tilde{A}Cq_0+\tilde{p}_0\tilde{B}Dp_0/M+2\tilde{q}_0\tilde{C}Bp_0).$$

(139)

The final wave packet is thus obtained from the initial wave packet at t_0 by multiplication by the phase factor $\exp\left[\frac{iS_{cl}(t,t_0)}{\hbar}\right]$ and by replacing the central position q_0, the initial momentum p_0 and the initial complex width parameters X_0, Y_0 in phase space (all of which are matrices) by their values at time t given by the $ABCD$ transformation law:

$$\begin{pmatrix} q_1 \\ p_1/M \end{pmatrix} = \begin{pmatrix} A & B \\ C & D \end{pmatrix}\begin{pmatrix} q_0 \\ p_0/M \end{pmatrix} + \begin{pmatrix} \xi \\ n\dot{\xi} \end{pmatrix} \quad (140)$$

$$\begin{pmatrix} X \\ Y \end{pmatrix} = \begin{pmatrix} A & B \\ C & D \end{pmatrix}\begin{pmatrix} X_0 \\ Y_0 \end{pmatrix}. \quad (141)$$

As both sides can be expanded in increasing powers of α with 3D Hermite-Gauss functions as coefficients, the theorem is proved for all modes of propagation.

If both the field gradient γ and the wave packet diffraction are neglected, the propagator for each internal state α reduces to the simplified classical form

$$\mathcal{K}_{\alpha,p_0}(q,q',t,t_0) = \exp\left[-\frac{i}{\hbar}\left(E_\alpha-\frac{\tilde{p}_0Bp_0}{2M_\alpha}\right)-\right.$$

$$\left.\frac{iM_\alpha}{2\hbar}\int_{t_0}^t \widetilde{\dot{\xi}}(t_1,t_0)n\dot{\xi}(t_1,t_0)\mathrm{d}t_1\right]$$

$$\exp\left[\frac{iM_\alpha}{\hbar}\widetilde{\dot{\xi}}(t,t_0)nq\right]$$

$$\delta[q-q'-Bp_0/M_\alpha-\xi(t,t_0)],$$

(142)

with $B = \int_{t_0}^t n^{-1}(t_1)\mathrm{d}t_1$, which generalizes the propagator used to recover the classical approximation in previous papers.

Appendix 3

Explicit quantum mechanical calculation of the fringes in a fountain atomic clock

The goal of this appendix is to illustrate the calculation of the excited state amplitude by the $ABCD\xi$ formalism in the simple case of an atomic fountain clock. The fringes result from the interference of atom waves propagating along two different external paths entangled with the state of internal excitation of the atoms $\alpha = a,b$. The excited state amplitude of atoms in a fountain is given by

$$< \vec{r},b \mid \Psi(t) > = \int \mathrm{d}^3r_1\mathrm{d}^3r_1'\mathrm{d}^3r_0\mathcal{K}_b(\vec{r},\vec{r}_1,t,t_1)$$

$$< \vec{r}_1,b \mid \mathcal{T}\exp\left[-\frac{i}{\hbar}\int_{t_0}^t \mathrm{d}t'\widetilde{V}(\vec{r}_{op},\overrightarrow{p}_{op},t')\right] \mid \vec{r}_1',a >$$

$$\mathcal{K}_a(\vec{r}_1',\vec{r}_0,t_1,t_0) < \vec{r}_0,a \mid \Psi(t_0) >,$$

(143)

where the free propagators $\mathcal{K}_\alpha(\vec{r}, \vec{r}_1, t, t_1)$ are given in the text and where

$$< \vec{r}_1, b \mid \mathcal{T} \exp\left[-\frac{i}{\hbar}\int_{t_0}^{t} \mathrm{d}t' \widetilde{V}(\vec{r}_{op}, \vec{p}_{op}, t')\right] \mid \vec{r}_1', a >$$

$$= < \vec{r}_1, b \mid \mathcal{T} \exp\left[-\frac{i}{\hbar}\int_{t_0}^{t} \mathrm{d}t' \hat{V}(\vec{R}_{op}(t', t_1), t')\right] \mid \vec{r}_1', a > \tag{144}$$

is the transfer matrix element of the interaction Hamiltonian for each field zone (in the interaction representation $\hat{V} = e^{iH_0(t-t_1)} V e^{-iH_0(t-t_1)}$ in the absence of spin-rotation interaction).[12] In the magnetic dipole approximation, this matrix element is given to first order by

$$\frac{i}{\hbar}\int_{t_0}^{t} \mathrm{d}t' < b \mid \widetilde{\vec{\mu}}_{op}(t' - t_1) \mid a >$$

$$\frac{1}{(2\pi)^{3/2}}\int \mathrm{d}^3 k\, e^{i\vec{k}\cdot[\vec{r}_1 - \vec{r}_0 + \vec{\xi}(t', t_1)]} e^{i\frac{\hbar k^2}{2M}(t' - t_1)} \vec{\mathcal{B}}(\vec{k}, t')$$

$$\delta\left[\vec{r}_1 - \vec{r}_1' + \frac{\hbar \vec{k}}{M}(t' - t_1)\right], \tag{145}$$

which leads to the following expression of the main text, when the effect of gravitation is neglected in the interaction zone (with $k_z = \pm k$):

$$b_\pm^{(1)}(\vec{r}, t)$$

$$= i\sqrt{\pi} e^{i(\pm kz - \omega t + \varphi)} \int \frac{\mathrm{d}^3 p}{(2\pi\hbar)^{3/2}} \frac{w\Omega_{ba}}{v_x}$$

$$e^{-w^2(\omega - \omega_{ba} \mp kv_z - \delta)^2/4v_x^2}$$

$$e^{i(\omega - \omega_{ba} \mp kv_z - \delta)(x - x_1)/v_x}$$

$$e^{i[\vec{p}\cdot(\vec{r} - \vec{r}_0) - E_a(\vec{p})(t - t_0)]/\hbar} a^{(0)}(\vec{p}). \tag{146}$$

For strong field expressions of the e.m. interaction matrix element with various field profiles, see [15, 13, 42, 38, 43] and the recent analysis in [18] for microwave clocks.

Here, for simplicity, we restrict ourselves to a two-dimensional problem, x for the vertical direction and z for the transverse direction of propagation of the microwave field.

If the initial wave packet $< \vec{r}, a \mid \Psi(t_0) >$ in the internal state a is centred at the vertical position $x_c(t_0)$

at time t_0 and is considered, momentarily, as a plane wave in the tranverse direction z, it can be written

$$F(x - x_c(t_0), X(t_0), Y(t_0))$$
$$\exp[iM_a v_x(t_0)[x - x_c(t_0)]/\hbar]\exp[iM_a v_z z/\hbar]. \tag{147}$$

The propagated wave packet at time t_1 at the vertical position x_1 and transverse position z_1 is

$$\int \mathrm{d}x_0 \mathrm{d}z_0 \mathcal{K}_a(x_1, z_1, x_0, z_0, t_1, t_0)$$
$$F(x_0 - x_c(t_0), X(t_0), Y(t_0))$$
$$\exp[iM_a v_x(t_0)[x_0 - x_c(t_0)]/\hbar]$$
$$\exp[iM_a v_z z_0/\hbar]$$
$$= \exp[iS_a(t_1, t_0)/\hbar]$$
$$\exp\{iM_a v_x(t_1)[x_1 - x_c(t_1)]/\hbar\}$$
$$\exp\{iM_a v_z[z_1 - v_z(t_1 - t_0)]/\hbar\}$$
$$F(x - x_c(t_1), X(t_1), Y(t_1)), \tag{148}$$

where

$$x_c(t_1) = A(t_1, t_0)x_c(t_0) +$$
$$B(t_1, t_0)v_x(t_0) + \xi(t_1, t_0) \tag{149}$$
$$v_x(t_1) = C(t_1, t_0)x_c(t_0) +$$
$$D(t_1, t_0)v_x(t_0) + \dot{\xi}(t_1, t_0), \tag{150}$$

and where

$$S_a(t_1, t_0) = M_a \dot{\xi}(t_1, t_0)x_c(t_1) - \frac{M_a}{2}\int_{t_0}^{t_1}$$
$$[\dot{\xi}^2(t', t_0) + \gamma\xi^2(t', t_0)]\mathrm{d}t' - E_a(t_1 - t_0) +$$
$$\frac{M_a}{2}[ACx_c^2(t_0) + DBv_x^2(t_0) +$$
$$v_z^2(t_1 - t_0) + 2BCx_c(t_0)v_x(t_0)] \tag{151}$$

is the action calculated along the classical trajectory.

If x_A is the central position of the electromagnetic field zone, the effect of the interaction in the beam splitter is to multiply this wave packet by the transition amplitude factor

$$M_{ba} e^{i(\pm kz - \omega t_1 + \varphi)} e^{ik_x(x - x_A)} \tag{152}$$

with

$$k_x = (\omega - \omega_{ba}(v) \mp kv_z - \delta)/v_x. \tag{153}$$

The expression of the wave packet becomes

$$M_{ba} e^{-i(\omega t_1 - \varphi)} \exp\{ik_x[x_c(t_1) - x_A]\}$$
$$\exp(\pm ikz_1)\exp\left[\frac{iS_a(t_1, t_0)}{\hbar}\right]$$
$$\exp\{i[M_a v_x(t_1) + \hbar k_x][x_1 - x_c(t_1)]/\hbar\}$$
$$\exp\{iM_a v_z[z_1 - v_z(t_1 - t_0)]/\hbar\}$$
$$F(x_1 - x_c(t_1), X(t_1), Y(t_1)). \tag{154}$$

---

12. From Appendix 2, we have generally:
$\vec{R}_{op}(t) = A \cdot \vec{r}_{op} + B \cdot \vec{p}_{op}/M + \vec{\xi}(t, t_1)$, which reduces to $\vec{r}_{op} + \vec{p}_{op}(t - t_1)/M + \vec{\xi}(t, t_1)$ in the absence of rotation and field gradient.

After the interaction, at a later time t, the wave packet centre coordinate and the corresponding velocity are[13]

$$x_c(t) = A(t,t_1)x_c(t_1) + [B(t,t_1)/M_b]$$
$$(M_a v_x(t_1) + \hbar k_x) + \xi(t,t_1) \quad (155)$$
$$v_x(t) = C(t,t_1)x_c(t_1) + [D(t,t_1)/M_b]$$
$$(M_a v_x(t_1) + \hbar k_x) + \dot{\xi}(t,t_1) \quad (156)$$

and the relevant action is

$$S_b(t,t_1) = M_b \dot{\xi}(t,t_1)x_c(t) -$$
$$\frac{M_b}{2}\int_{t_1}^{t}[\dot{\xi}^2(t',t_1) + \gamma\xi^2(t',t_1)]\mathrm{d}t' +$$
$$\frac{1}{2M_b}(M_a v_z \pm \hbar k)^2(t-t_1) +$$
$$\frac{M_b}{2}\left\{ACx_c^2(t_1) + \frac{DB}{M_b^2}[M_a v_x(t_1) + \hbar k_x]^2 +\right.$$
$$\left. 2\frac{BC}{M_b}x_c(t_1)[M_a v_x(t_1) + \hbar k_x]\right\} - E_b(t-t_1). \quad (157)$$

The final expression of the wave packet becomes

$$M_{ba}e^{-i(\omega t_1 - \varphi)}\exp\{ik_x[x_c(t_1) - x_A]\}$$
$$\exp\left[\frac{iS_b(t,t_1)}{\hbar}\right]\exp\left[\frac{iS_a(t_1,t_0)}{\hbar}\right]$$
$$\exp\left\{\frac{iM_b}{\hbar}v_x(t)[x - x_c(t)]\right\}$$
$$\exp\{i(M_a v_z \pm \hbar k)[z - (1/M_b)(M_a v_z \pm \hbar k)(t-t_1)] - iM_a v_z^2(t_1-t_0)/\hbar\}F(x - x_c(t), X(t), Y(t)). \quad (158)$$

In the special case where $\gamma = 0, A = D = 1, C = 0, B(t,t_1) = t - t_1, B(t_1,t_0) = t_1 - t_0$, the previous expression simplifies to[14]

$$M_{ba}e^{-i(\omega t_1 - \varphi)}\exp\{ik_x[x_c(t_1) - x_A]\}$$
$$\exp\left[\frac{iM_b}{\hbar}\dot{\xi}(t,t_1)x_c(t) - \frac{iM_b}{2\hbar}\int_{t_1}^{t}\dot{\xi}^2(t',t_1)\mathrm{d}t'\right]$$
$$\exp\left[\frac{i}{2\hbar}\left(\frac{1}{M_b}\left\{M_a\left[v_x(t_0) + \dot{\xi}(t_1,t_0)\right] +\right.\right.\right.$$
$$\left.\left.\left.\hbar k_x\right\}^2(t-t_1)\right) - \frac{i}{\hbar}E_b(t-t_1)\right]$$
$$\exp\left[\frac{iM_a}{\hbar}\dot{\xi}(t_1,t_0)x_c(t_1)\right]$$

13. Rigorously, the $ABCD$ transformation law, which originates from a Hamiltonian formalism developed in [16], should be used as an $A(MB)(C/M)D$ law for the position/momentum pair.
14. In a rotating frame, B is the matrix $\mathcal{R}(t,t_1)B_0(t,t_1)$, which leads to a Sagnac effect through terms such as $\exp\left[ik_x\Omega_y v_z(t-t_1)^2\right]$, and to a Sagnac shift for an asymmetric v_z distribution and unequal travelling wave intensities.

$$\exp\left[-\frac{iM_a}{2\hbar}\int_{t_0}^{t_1}\dot{\xi}^2(t',t_0)\mathrm{d}t' +\right.$$
$$\left.\frac{iM_a}{2\hbar}v_x^2(t_0)(t_1 - t_0) - \frac{i}{\hbar}E_a(t_1 - t_0)\right]$$
$$\exp\left[\frac{i}{\hbar}\left\{M_a\left[v_x(t_0) + \dot{\xi}(t_1,t_0)\right] + \hbar k_x + M_b\dot{\xi}(t,t_1)\right\}\right.$$
$$\left[x - x_c(t_1) - (1/M_b)\left\{M_a\left[v_x(t_0) + \dot{\xi}(t_1,t_0)\right] + \hbar k_x\right\}\right.$$
$$(t - t_1) - \xi(t,t_1)\Big]$$
$$F(x - x_c(t), X(t), Y(t)) \quad (159)$$

multiplied by the same factor for the z direction:

$$\exp\left[\frac{i}{2\hbar}\frac{1}{M_b}(M_a v_z \pm \hbar k)^2(t - t_1)\right]$$
$$\exp\left[\frac{iM_a}{2\hbar}v_z^2(t_1 - t_0)\right]$$
$$\exp\{i(M_a v_z \pm \hbar k)[z - (1/M_b)(M_a v_z \pm \hbar k)(t-t_1)] - iM_a v_z^2(t_1 - t_0)/\hbar\}. \quad (160)$$

We use this expression for both arms with the following sequences:

- on arm 1, a first interaction at time t_1, where t_1 is chosen such that $x_c(t_1) = x_A$, so that we let $t_0 = t_1$ in the previous expression:

$$b_{1+}(x,z,t) = M_{ba}e^{-i(\omega t_1 - \varphi_1)}$$
$$\exp\left[\frac{iM_b}{\hbar}\dot{\xi}(t,t_1)x_c(t) - \frac{iM_b}{2\hbar}\int_{t_1}^{t}\dot{\xi}^2(t',t_1)\mathrm{d}t'\right]$$
$$\exp\left[\frac{i}{2\hbar}\left\{\frac{1}{M_b}[(M_a v_x + \hbar k_x)^2 +\right.\right.$$
$$\left.\left.(M_a v_z + \hbar k)^2](t - t_1)\right\} - \frac{i}{\hbar}E_b(t - t_1)\right]$$
$$\exp\left[\frac{i}{\hbar}[M_a v_x + \hbar k_x + M_b\dot{\xi}(t,t_1)]\right]$$
$$[x - x_A - (1/M_b)(M_a v_x + \hbar k_x)(t - t_1) - \xi(t,t_1)]$$
$$\exp\{i(M_a v_z + \hbar k)[z - (1/M_b)(M_a v_z + \hbar k)(t-t_1)]/\hbar\}$$
$$F(x - x_c(t), X(t), Y(t)), \quad (161)$$

with $v_x(t_1) = v_x$;

- on arm 2, we replace t_0 by t_1 as the initial time and the second interaction takes place at a later time t_2:

$$b_{2\pm}(x,z,t_2) = M_{ba}e^{-i(\omega t_2 - \varphi_2)}$$
$$\exp[ik_x'(x - x_B)]\exp[\pm ikz]$$
$$\exp\left[\frac{iM_a}{\hbar}\dot{\xi}(t_2,t_1)x_c'(t_2)\right]$$
$$\exp\left[-\frac{iM_a}{2\hbar}\int_{t_1}^{t_2}\dot{\xi}^2(t',t_1)\mathrm{d}t'\right]$$

$$\exp\left[\frac{iM_a}{2\hbar}[v_x^2 + v_z'^2](t_2 - t_1) - \frac{i}{\hbar}E_a(t_2 - t_1)\right]$$

$$\exp\left(\frac{i}{\hbar}\left\{M_a\left[v_x + \dot{\xi}(t_2, t_1)\right]\right\}[x - x_c'(t_2)]\right)$$

$$\exp\{iM_a v_z'[z - v_z'(t_2 - t_1)]/\hbar\}$$

$$F(x - x_c'(t_2), X(t_2), Y(t_2)), \tag{162}$$

where t_2 is chosen such that the centre of the wave packet on arm 2 coincides with the position of the second interaction:

$$x_c'(t_2) = x_A + v_x(t_2 - t_1) + \xi(t_2, t_1) = x_B. \tag{163}$$

If $x_A = x_B$ (single microwave resonator) this implies that $v_x(t_2 - t_1) = -\xi(t_2, t_1)$. For a constant acceleration g, $\xi(t_2, t_1) = -\frac{1}{2}g(t_2 - t_1)^2$ and hence $(t_2 - t_1) = 2v_x/g$. At the same time t_2, the first wave-packet centre is at position

$$x_c(t_2) = x_A + (1/M_b)(M_a v_x + \hbar k_x)(t_2 - t_1) + \xi(t_2, t_1), \tag{164}$$

which differs from the previous one by[15]

$$\Delta x = x_c(t_2) - x_c'(t_2) = \left(\frac{M_a}{M_b} - 1\right)\frac{2v_x^2}{g} + \frac{2\hbar k_x}{M_b g}v_x. \tag{166}$$

The wave-packet velocities are then respectively

$$v_x(t_2) = (1/M_b)(M_a v_x + \hbar k_x) + \dot{\xi}(t_2, t_1)$$
$$\simeq -v_x + \hbar k_x/M_b \tag{167}$$

$$v_x'(t_2) = \left(M_a v_x + M_a\dot{\xi}(t_2, t_1) + \hbar k_x'\right)/M_b$$
$$= -(M_a v_x + \hbar k_x)/M_b, \tag{168}$$

with

$$k_x' = -[\omega - \omega_{ba}(v) \mp kv_z - \delta]/v_x = -k_x \tag{169}$$

(energy conservation in the second interaction). This corresponds to a difference in kinetic energy precisely equal to the difference in potential energy:

$$M_b g \Delta x = \frac{M_b v_x'^2}{2} - \frac{M_b v_x^2}{2}. \tag{170}$$

---

15. If we approximate g by

$$GM_\oplus/R_\oplus^2$$

then

$$\frac{2\hbar k_x}{M_b g}v_x = 2\left(\frac{\hbar c}{Gm_p^2}\right)\frac{m_p}{M_\oplus}\frac{m_p}{M_b}k_x R_\oplus^2\frac{v_x}{c}, \tag{165}$$

where $\hbar c/G$ is the square of the Planck mass, m_p the proton mass, $M_\oplus$ the mass of the Earth and $R_\oplus$ its radius. The Planck mass appears here as in any problem where the ratio of $\hbar$ and g is involved (e.g. the watt balance or atomic Bloch oscillations).

We can now calculate the interference term in the excited state population at time t_2:

$$b_{1+}(x, z, t_2)b_{2\pm}^*(x, z, t_2) =$$
$$M_{ba}M_{ba}^* e^{i(\omega t_2 - \varphi_{2\pm})}e^{-i(\omega t_1 - \varphi_{1+})}$$
$$\exp(-ik_x'(x - x_B))$$
$$\exp(\mp ikz)\exp\left[\frac{i}{\hbar}(E_a - E_b)(t_2 - t_1)\right]$$
$$\exp\left[\frac{i}{\hbar}(M_b - M_a)\dot{\xi}(t_2, t_1)x - \frac{i}{2\hbar}(M_b - M_a)\int_{t_1}^{t_2}\dot{\xi}^2(t', t_1)dt'\right]$$
$$\exp\left\{\frac{i}{2\hbar}\left[\frac{1}{M_b}(M_a v_x + \hbar k_x)^2(t_2 - t_1) - M_a v_x^2(t_2 - t_1)\right]\right\}$$
$$\exp\left\{\frac{i}{2\hbar}\left[\frac{1}{M_b}(M_a v_z + \hbar k)^2(t_2 - t_1) - M_a v_z'^2(t_2 - t_1)\right]\right\}$$
$$\exp\left\{\frac{i}{\hbar}(M_a v_x + \hbar k_x)[x - x_A - (1/M_b)(M_a v_x + \hbar k_x)(t_2 - t_1) - \xi(t_2, t_1)]\right\}$$
$$\exp\left\{-\frac{i}{\hbar}M_a v_x[x - x_A - v_x(t_2 - t_1) - \xi(t_2, t_1)]\right\}$$
$$\exp\{i(M_a v_z + \hbar k)[z - (1/M_b)(M_a v_z + \hbar k)(t_2 - t_1)]/\hbar\}$$
$$\exp\{-iM_a v_z'[z - v_z'(t_2 - t_1)]/\hbar\}$$
$$F(x - x_c(t_2), X(t_2), Y(t_2))$$
$$F^*(x - x_c'(t_2), X(t_2), Y(t_2)). \tag{171}$$

From the expression of k_x resulting from energy conservation, the time-dependent phase factor

$$\exp\left[i(\omega - \omega_{ba} + \omega_{ba}\frac{M_a}{M_b}\frac{v^2}{2c^2} - \frac{M_a}{M_b}kv_z - \frac{M_a}{M_b}k_x v_x - \frac{\hbar k^2}{2M_b})(t_2 - t_1)\right] \tag{172}$$

disappears and

$$b_{1+}(x, z, t_2)b_{2\pm}^*(x, z, t_2) =$$
$$M_{ba}M_{ba}^* \exp[ik_x(x - x_A)]\exp[-ik_x'(x - x_B)]$$
$$\exp(ikz \mp ikz)\exp[iM_a(v_z - v_z')z/\hbar]$$
$$\exp\left[-\frac{iM_a}{2\hbar}(v_z^2 - v_z'^2)(t_2 - t_1)\right]$$
$$\exp\left[\frac{i}{\hbar}(M_b - M_a)\dot{\xi}(t_2, t_1)x - \frac{i}{2\hbar}(M_b - M_a)\int_{t_1}^{t_2}\dot{\xi}^2(t', t_1)dt'\right]$$

$$\exp[-ik_x\xi(t_2,t_1)]$$
$$F(x - x_c(t_2), X(t_2), Y(t_2))$$
$$F^*(x - x'_c(t_2), X(t_2), Y(t_2)), \qquad (173)$$

in which we have the expected spatial beat owing to the difference in momentum of the two wave packets. At this point, it is convenient to introduce a wave-packet structure G in z (F is a plane wave component of G) and after v_z and v'_z integration, the previous expression becomes

$$b_{1+}(x, z, t_2)b_{2\pm}^*(x, z, t_2) =$$
$$M_{ba}M_{ba}^* \exp[i\kappa_x(x - x_A)]\exp[-i\kappa'_x(x - x_B)]$$
$$\exp(ikz \mp ikz)$$
$$\exp\left[\frac{i}{\hbar}(M_b - M_a)\dot{\xi}(t_2,t_1)x - \right.$$
$$\frac{i}{2\hbar}(M_b - M_a)\int_{t_1}^{t_2}\dot{\xi}^2(t', t_1)\mathrm{d}t'\right]$$
$$\exp[-i\kappa_x\xi(t_2,t_1)]$$
$$G\left(z - \frac{\hbar k}{M_a v_x}[x - x_A - \xi(t_2,t_1)],\right.$$
$$x - x_c(t_2), X(t_2), Y(t_2)\right)$$
$$G^*\left(z \mp \varepsilon\frac{\hbar k}{M_a v_x}(x - x_B),\right.$$
$$\left. x - x'_c(t_2), X(t_2), Y(t_2)\right), \qquad (174)$$

with

$$\kappa_x = \varepsilon\kappa'_x = [\omega - \omega_{ba}(v) - \delta]/v_x, \qquad (175)$$

where $\varepsilon = 1$, $\xi = 0$, $x_A = x_1$, $x_B = x_2$, in the absence of gravity and where $\varepsilon = -1$, $x_A = x_B$, in the case of the fountain with a single resonator.

Finally, we can integrate the previous signal over space coordinates z and x. For this, we use the same formula:

$$\int_{-\infty}^{+\infty} \exp\left[-P(z-a)^2\right]\exp\left[-P^*(z-b)^2\right]$$
$$\exp\left[i\frac{Mv}{\hbar}(z-a)\right]\exp\left[-i\frac{Mv'}{\hbar}(z-b)\right]\mathrm{d}z$$
$$= \frac{\sqrt{\pi}}{\sqrt{P+P^*}}\exp\left[-\frac{PP^*}{P+P^*}(a-b)^2 - \right.$$
$$\left.\frac{K^2}{P+P^*} - \frac{2K(a-b)\mathrm{Im}P}{P+P^*}\right]$$
$$\exp[iK(a+b)]\exp\left[i\frac{M(v'b - va)}{\hbar}\right], \qquad (176)$$

with $2K = M(v - v')/\hbar$, from which we infer incidentally the following theorem:

The phase factor resulting from the velocity difference after integration is equal to the phase factor calculated at the mid-point $z = (a + b)/2$ before integration:

$$\exp[iK(a+b)]\exp\left[i\frac{M(v'b - va)}{\hbar}\right] =$$
$$\exp\left[i\frac{Mv}{\hbar}\left(\frac{a+b}{2} - a\right)\right]\exp\left[-i\frac{Mv'}{\hbar}\left(\frac{a+b}{2} - b\right)\right]. \qquad (177)$$

With the previous integral we find

$$\int_{-\infty}^{+\infty} \exp\left\{-P\left[z - \frac{\hbar k}{M_a v_x}(x - x_A - \xi)\right]^2\right\}$$
$$\exp\left\{-P^*\left[z \mp \varepsilon\frac{\hbar k}{M_a v_x}(x - x_B)\right]^2\right\}$$
$$\exp[(1 \pm 1)ikz]\mathrm{d}z$$
$$= \Delta z\sqrt{2\pi}\sqrt{1 + T^2}\exp\left[-(1 \pm 1)k^2(\Delta z)^2\right]$$
$$\exp\left\{i\frac{\hbar k^2}{M_a v_x}\frac{1 \mp 1}{2}[x(1 \pm \varepsilon) - (x_A \pm \varepsilon x_B) - \xi]\right\}$$
$$\exp\left\{-\frac{1}{8(\Delta z)^2}\left(\frac{\hbar k}{M_a v_x}\right)^2[x(1 \mp \varepsilon) - (x_A \mp \varepsilon x_B) - \right.$$
$$\left. \xi + (1 \mp 1)v_x(t - t_0)]^2\right\}, \qquad (178)$$

with

$$P = \frac{1}{4(\Delta z)^2(1 + iT)} \qquad (179)$$

and $T = \hbar(t - t_0)/2M_a(\Delta z)^2$ where t_0 is the time for which the wave packet has its minimum z uncertainty.

The x integral can be performed in the same manner or we may use the previous mid-point theorem to discuss phase shifts directly.

Finally, from the final probability formula (174), we keep the following phase factors:

$$\exp[-i(\omega - \omega_{ba}^0 - \delta)\xi(t_2,t_1)/v_x], \qquad (180)$$

which gives the main phase factor for the Ramsey fringes;

$$\exp\left[i\frac{2\delta}{v_x}\frac{1 \mp 1}{2}[x(1 \pm \varepsilon) - (x_A \pm \varepsilon x_B) - \xi]\right], \quad (181)$$

which gives a correction to the recoil shift associated with each contribution;

$$\exp\left[\frac{i}{\hbar}(M_b - M_a)\dot{\xi}(t_2,t_1)x\right], \qquad (182)$$

which gives the global gravitational red shift of the fountain and the remaining phase factors give the

right combination of the relativistic Doppler shift and gravitational phase shift corrections:

$$\exp\left[-i\omega_{ba}^0\left(\frac{v_x^2}{2c^2}\right)\frac{\xi(t_2,t_1)}{v_x}-\right.$$
$$\left.i\frac{\omega_{ba}^0}{2c^2}\int_0^{2v_x/g}(gt')^2\mathrm{d}t'\right]$$
$$=\exp\left[i\omega_{ba}^0\left(\frac{v_x^2}{2c^2}\right)\frac{2v_x}{g}-i\frac{\omega_{ba}^0}{2c^2}\frac{g^2}{3}\left(\frac{2v_x}{g}\right)^3\right]$$
$$=\exp\left\{-i\left[\omega_{ba}^0\left(\frac{v_x^2}{6c^2}\right)\frac{2v_x}{g}\right]\right\}. \qquad (183)$$

We should also emphasize that there is a contrast factor owing to the vertical separation of the wave packets $x_c(t_2)-x_c'(t_2)$, for which we have seen that the Planck mass was directly involved.

References

1. Berman P. (ed.), *Atom Interferometry*, New York, Academic Press, 1997.
2. Bordé Ch. J., In *Laser Spectroscopy* (Edited by R. Blatt, J. Eschner, D. Leibfried and F. Schmidt-Kaler), Singapore, World Scientific, 1999, 160-169; *idem*, Relativistic quantum theory of microwave and optical atomic clocks, In *Frequency Standards and Metrology* (Edited by P. Gill), Singapore, World Scientific, 2002, 18-25; *idem*, Atomic Clocks and Atom Interferometry, In *Advances in the Interplay between Quantum and Gravity Physics* (Edited by V. de Sabbata), Dordrecht, Kluwer Academic Publishers, 2002, 27-55.
3. Bloch I., Hänsch T. W., Esslinger T., *Nature*, 2000, **403**, 166-170 and references therein.
4. Bloch I., Hänsch T. W., Esslinger T., *Phys. Rev. Lett.*, 1999, **82**, 3008-3011.
5. Gerbier F., Bouyer P., Aspect A., *Phys. Rev. Lett.*, 2001, **87**, 4729-4733 and references therein.
6. Le Coq Y., Thywissen J. H., Rangwala S. A., Gerbier F., Richard S., Delannoy G., Bouyer P., Aspect A., *Phys. Rev. Lett.*, 2001, **87**, 170403.
7. Bordé Ch. J., *Phys. Lett. A*, 1995, **204**, 217-222; *idem*, In *Laser Spectroscopy* (Edited by M. Inguscio, M. Allegrini and A. Sasso), Singapore, World Scientific, 303-307, 1996; *idem*, *Ann. Phys.*, 1995, **20**, 477-485.
8. Lemonde P. et al., In *Frequency measurement and control* (Edited by A. N. Luiten), *Topics Appl. Phys.*, 2001, **79**, 131-152, Berlin, Springer-Verlag.
9. Grad H., *Commun. Pure Appl. Math.*, 1949, **2**, 325.
10. Bordé Ch. J., Propagation of laser beams and of atomic systems, Les Houches Lectures, Session LIII, 1990, *Fundamental Systems in Quantum Optics* (Edited by J. Dalibard, J.-M. Raimond and J. Zinn-Justin), New York, Elsevier Science, 1991, 287-380.
11. Bordé Ch. J., Hall J. L., Kunasz C. V., Hummer D. G., *Phys. Rev.*, 1976, **14**, 236-263.
12. Sterr U., Sengstock K., Ertmer W., Riehle F., Helmcke J., Atom interferometry based on separated light fields, in [1], 293-362.
13. Bordé Ch. J., Courtier N., du Burck F., Goncharov A. N., Gorlicki M., *Phys. Lett. A*, 1994, **188**, 187-197.
14. Sterr U., Sengstock K., Müller J. H., Bettermann D., Ertmer W., *Appl. Phys. B*, 1992, **54**, 341.
15. Ishikawa J., Riehle F., Helmcke J., Bordé Ch. J., *Phys. Rev. A*, 1994, **49**, 4794-4825.
16. Bordé Ch. J., *C. R. Acad. Sci. Paris*, 2001, t. 2, Série IV, 509-530.
17. Bordé Ch. J., Conference given at the Symposium on the occasion of the 125th anniversary of the metric convention, Paris, 2000.
18. Wolf P. et al., *Proc. 2001 IEEE Frequency Control Symposium*, Seattle, USA, 2001, 37-45.
19. Landau L. D., Lifschitz E. M., *Quantum Mechanics*, London, Pergamon Press.
20. Wallis H., Dalibard J., Cohen-Tannoudji C., *Appl. Phys. B*, 1992, **54**, 407-419.
21. Berthoud P., Fretel E., Joyet A., Dudle G., Thomann P., *IEEE Trans. Instrum. Meas.*, 1999, **48**, 516-519.
22. Bordé Ch. J., *C. R. Acad. Sci. Paris*, 1977, **284B**, 101-104; *idem*, In *Laser Spectroscopy III*, Berlin, Springer-Verlag, 1977.
23. Bordé Ch. J., *Phys. Lett.*, 1989, **A140**, 10-12.
24. Bordé Ch. J., In *Laser Spectroscopy X*, Singapore, World Scientific, 1991, 239-245.
25. Bordé Ch. J., Weitz M., Hänsch T. W., In *Laser Spectroscopy* (Edited by L. Bloomfield, T. Gallagher and D. Larson), New York, American Institute of Physics, 1994, 76-78.
26. Weiss D. S., Young B. C., Chu S., *Appl. Phys. B*, 1994, **59**, 217-256.
27. Young B. C., Kasevich M., Chu S., Precision atom interferometry with light pulses, in [1], 363-406, and references therein; Wicht A., Hensley J. M., Sarajlic E., Chu S., In *Frequency Standards and Metrology* (Edited by P. Gill), Singapore, World Scientific, 2002, 193-212.
28. Bordé Ch. J., Avrillier S., van Lerberghe A., Salomon Ch., Bréant Ch., Bassi D., Scoles G., *Appl. Phys. B*, 1982, **28**, 82; *idem*, *Jour. Phys. Coll.*, 1981, **42**, C8-15-C8-19.
29. Trebst T., Binnewies T., Helmcke J., Riehle F., *IEEE Trans. Instrum. Meas.*, 2001, **50**, 535-538 and references therein.
30. Udem Th. et al., *Phys. Rev. Lett.*, 2001, **86**, 4996.
31. Oates C. W., Curtis E. A., Hollberg L., *Opt. Lett.*, 2000, **25**, 1603.
32. Hollberg L., Oates C. W., Curtis E. A., Ivanov E. N., Diddams S. A., Udem Th., Robinson H. G., Bergquist J. C., Rafac R. J., Itano W. M., Drullinger R. E., Wineland D. J., *IEEE J. Quantum Electron.*, to be published, and references therein.
33. In *Frequency Standards and Metrology* (Edited by P. Gill), Singapore, World Scientific, 2002: Riehle F., Wilpers G., Sterr U., Binnewies T., Helmcke J., 339-346; and Curtis E. A., Oates C. W., Diddams S. A., Udem Th., Hollberg L., 331-338.
34. Hall J. L., Bordé Ch. J., Uehara K., *Phys. Rev. Lett.*, 1976, **37**, 1339.

35. Heupel T., Mei M., Niering M., Gross B., Weitz M., Hänsch T. W., Bordé Ch. J., *Europhys. Lett.*, 2002, **57**, 158-163.

36. Bordé Ch. J., *Revue du Cethedec – Ondes et Signal*, 1983, **NS83-1**, 1-118; Erratum No. 76, 191.

37. Bordé Ch. J., Salomon Ch., Avrillier S., van Lerberghe A., Bréant Ch., Bassi D., Scoles G., *Phys. Rev. A*, 1984, **30**, 1836-1848.

38. Lämmerzahl C., Bordé Ch. J., *Phys. Lett. A*, 1995, **203**, 59-67.

39. Marzlin K.-P., Audretsch J., *Phys. Rev. A*, 1996, **53**, 1004.

40. Rauch H., Petrascheck D., In *Neutron Diffraction* (Edited by H. Dachs), Berlin, Springer-Verlag, 1978, 303-351 and references therein.

41. Bordé Ch. J., Matter-wave interferometers: a synthetic approach, in [1], 257-292.

42. Bordé Ch. J., Lämmerzahl C., *Ann. Physik (Leipzig)*, 1999, **8**, 83-110.

43. Lämmerzahl C., Bordé Ch. J., *General Relativity and Gravitation*, 1999, **31**, 635.

44. Bordé Ch. J., Houard J.-C., Karasiewicz A., In *Gyros, Clocks and Interferometers: Testing Relativistic Gravity in Space* (Edited by C. Lämmerzahl, C. W. F. Everitt and F. W. Hehl), Berlin, Springer-Verlag, 2001, 403-438 and gr-qc/0008033.

45. Bordé Ch. J., Karasiewicz A., Tourrenc Ph., *Int. J. Mod. Phys. D*, 1994, **3**, 157-161.

46. Hehl F. W., Ni Wei-Tou, *Phys. Rev. D*, 1990, **42**, 2045-2048.

47. Gupta S. N., *Proc. Phys. Soc. A*, 1952, **65**, 161-169; *idem*, *Proc. Phys. Soc. A*, 1952, **65**, 608-619.

48. Feynman R. P., Morinigo F. B., Wagner W. G., *Feynman Lectures on Gravitation* (Edited by B. Hatfield), Reading, Mass., Addison-Wesley, 1995.

49. Barker B. M., Gupta S. N., Haracz R. D., *Phys. Rev.*, 1966, **149**, 1027 and references therein.

50. Thomas L. H., *Phil. Mag.*, 1927, **3**, 1-22.

51. Audretsch J., Marzlin K.-P., *J. Phys. II (France)*, 1994, **4**, 2073-2087.

52. Audretsch J., Marzlin K.-P., *Phys. Rev. A*, 1994, **50**, 2080.

53. DeWitt B. S., *Phys. Rev. Lett.*, 1966, **16**, 1092.

54. Papini G., *Nuovo Cimento*, 1967, **52B**, 136-140.

55. Linet B., Tourrenc P., *Can. J. Phys.*, 1976, **54**, 1129-1133.

56. Peters A., Chung K. Y., Chu S., *Nature*, 1999, **400**, 849; *idem*, *Metrologia*, 2001, **38**, 25-61.

57. Collela R., Overhauser A. W., Werner S. A., *Phys. Rev. Lett.*, 1975, **34**, 1472.

58. Kasevich M., Chu S., *Phys. Rev. Lett.*, 1991, **67**, 181-184.

59. Snadden M. J., McGuirk J. M., Bouyer P., Haritos K. G., Kasevich M. A., *Phys. Rev. Lett.*, 1998, **81**, 971-974.

60. For an early treatment of a gravitational wave detector using an atom interferometric gradiometer see: Bordé Ch. J., Sharma J., Tourrenc Ph., Damour Th., *J. Phys. Lett.*, 1983, **44**, L-983-990.

61. Riehle F., Kisters Th., Witte A., Helmcke J., Bordé Ch. J., *Phys. Rev. Lett.*, 1991, **67**, 177-180.

62. Landragin A., Gustavson T. L., Kasevich M. A., In *Laser Spectroscopy, Proc. 14th International Conference on Laser Spectroscopy* (Edited by R. Blatt, J. Eschner, D. Leibfried and F. Schmidt-Kaler), Singapore, World Scientific, 1999, 170-176.

63. Holleville D., Fils J., Petit P., Dimarcq N., Clairon A., Bouyer P., Bordé Ch., Salomon Ch., *J. Phys. IV (France)*, 2000, **10**, Pr8-171.

64. Bingham R. et al., *HYPER, Hyper-Precision Cold Atom Interferometry in Space*, Assessment Study Report, ESA-SCI, 2000, 10.

65. Phillips T. J., *Hyperfine Interactions*, 1996, **100**, 163-172.

66. Arnaud J. A., *Beam and Fiber Optics*, New York, Academic Press, 1976.